Activation of *Torpedo* Acetylcholine Receptors Expressed in Mouse Fibroblasts

Single Channel Current Kinetics Reveal Distinct Agonist Binding Affinities

STEVEN M. SINE, TONI CLAUDIO, and FRED J. SIGWORTH

From the Department of Cellular and Molecular Physiology, Yale University School of Medicine, New Haven, Connecticut 06510

ABSTRACT The experiments described examine single channel currents recorded through *Torpedo* acetylcholine receptor channels stably expressed by a mouse fibroblast cell line. Closed-duration histograms were constructed from currents elicited by 0.5–300 μM acetylcholine (ACh). The concentration dependence of closed durations is well described by a four-state linear scheme with the addition of open-channel block by ACh. Analysis of closed durations measured at low concentrations gives estimates of the rate of opening of doubly liganded receptors, β, the rate of dissociation of ACh from doubly liganded receptors, k_{-2}, and the rate of channel closing, α. The rate of ACh dissociation from singly liganded receptors, k_{-1}, is then deduced from closed-duration histograms obtained at intermediate ACh concentrations. With k_{-1}, k_{-2}, and β determined, the rates of ACh association, k_{+1} and k_{+2}, are estimated from fitting closed-duration histograms obtained over a range of high ACh concentrations. A complete set of rate constants is presented for three experimental conditions: (*a*) Ca^{2+}-free extracellular solution containing 1 mM free Mg^{2+} at 22°C, (*b*) Ca^{2+}-free solution at 12°C, and (*c*) extracellular Ca^{2+} and Mg^{2+}, both at 0.5 mM, at 22°C. For all three conditions the dissociation constant for the first agonist binding site is ~100-fold lower than that for the second site. The different affinities are due primarily to different dissociation rates. Both the association and dissociation rates depend strongly on temperature. At 22°C ACh associates at diffusion-limited rates, whereas at 12°C association is 30- to 60-fold slower. Also slowed at 12°C are β (4-fold), k_{-2} (3-fold), k_{-1} (25-fold), and α (15-fold). In contrast to the activation rate constants, those for ACh-induced block decrease only twofold between 22 and 12°C. Changing from a Ca^{2+}-free to a Ca^{2+}-containing extracellular solution does not affect k_{+1} and k_{+2}, but increases β (twofold) and decreases k_{-2}, k_{-1}, and α (all twofold). Spectral analysis of single channel currents supports the parameter estimates obtained from fitting the open- and closed-duration histograms, and improves resolution of brief channel blockages produced by ACh.

Address reprint requests to Dr. Steven M. Sine, Department of Cellular and Molecular Physiology, Yale University School of Medicine, 333 Cedar Street, New Haven, CT 06510.

J. GEN. PHYSIOL. © The Rockefeller University Press · 0022-1295/90/08/0395/43 $2.00
Volume 96 August 1990 395–437

INTRODUCTION

At the vertebrate motor endplate acetylcholine (ACh) binds to the acetylcholine receptor (AChR) and triggers opening of the AChR channel. Because milligram quantities of AChR can be purified from the *Torpedo* electric organ, present understanding of AChR subunit composition, functional localization, and three-dimensional structure comes largely from the *Torpedo* AChR, and future structural information will also probably come from the *Torpedo* AChR. Although site-directed mutagenesis and single-channel recording experiments have provided insight into the transmembrane folding of the subunits and those portions lining the channel wall in *Torpedo* (Imoto et al., 1988) and in mouse (Leonard et al., 1988), relatively little is known about the kinetic steps that underlie activation of the *Torpedo* AChR.

Receptor activation can be defined as those processes leading to opening of the channel (agonist binding and channel opening) and those restoring the resting channel (channel closing and agonist dissociation). These processes were first investigated by measuring the agonist dose–response curve at frog endplates (Adams, 1975; Dionne et al., 1978; Dreyer et al., 1978) and in *Torpedo* vesicles (Forman and Miller, 1988). These studies revealed apparent dissociation constants for the various agonists (~30 μM for ACh and ~400 μM for carbamylcholine) and Hill coefficients n_H of ~2.0, indicating that two molecules of agonist must bind to the AChR to open the channel. However, the molecular steps underlying the dose–response curve remained largely unknown until the advent of single-channel recording techniques. Recordings of single channels at low ACh concentrations revealed that the AChR channel opens within tens to hundreds of microseconds of binding agonist, depending on the source of the receptor studied (garter snake endplate: Dionne and Leibowitz, 1982; frog endplate: Colquhoun and Sakmann, 1985; BC3H-1 cells, a mouse muscle-like cell line: Sine and Steinbach, 1986), and that channel opening and ACh dissociation occur at similar rates. Measurements of the concentration dependence of single channel currents showed that ACh binds to the AChR at nearly diffusion-limited rates (Auerbach and Lingle, 1987; Sine and Steinbach, 1987; Colquhoun and Ogden, 1988). Thus, when the endplate is presented with a pulse of ACh, the ACh binds rapidly and the AChR channel opens with short latency. The open state persists for several milliseconds, but once the channel closes ACh dissociates so rapidly that it reopens on average only once before ACh dissociates.

The affinity of the two binding sites for agonists has been estimated from single channel recordings carried out over a range of high agonist concentrations. Measurements by Auerbach and Lingle (1987) and Sine and Steinbach (1987) are consistent with slight positive cooperativity in agonist binding to AChRs on BC3H-1 cells (dissociation constants 50 and 10 μM) and to 40-pS AChRs on *Xenopus* myotomes (66 and 7 μM), whereas those by Colquhoun and Ogden (1988) obtained at the frog endplate are consistent with identical binding affinities (77 μM at negative potentials). Jackson (1988) measured currents through AChRs from cultured rat muscle and found, in contrast, distinct agonist binding affinities (5 μM and 3.5 mM) for the agonist carbamylcholine.

It is well established that classical competitive antagonists bind to the two ACh binding sites with different affinity (Neubig and Cohen, 1979; Sine and Taylor,

1981). Since, for agonists, binding measurements reveal Hill coefficients near unity (Weiland and Taylor, 1979), and for some AChR preparations greater than unity (Weber and Changeux, 1974; Sine and Taylor, 1979), it might seem unlikely that the agonist would bind to the two sites with different affinity. However in these studies binding is measured at equilibrium, where some AChRs are activatable but most are desensitized. It is therefore possible that activatable receptors bind agonist with different affinities, but the affinity difference is not detected because the major AChR species is in the desensitized state.

Owing to the small size and tight packing of the cells in the *Torpedo* electric organ, single channel measurements have not been undertaken on the native *Torpedo* AChR. The present work takes advantage of the stable expression system developed by Claudio et al. (1987) in which clonal fibroblasts are stably transfected with the four genes coding for the *Torpedo* AChR. We use the patch clamp technique to examine activation of single *Torpedo* AChR channels over a wide range of ACh concentrations. The measurements are well described by a four-state linear scheme plus open channel block by ACh. Fitting the predictions of this scheme to the data discloses rate constants for each step in the activation pathway of *Torpedo* AChRs. The rate constants obtained reveal distinct agonist binding affinities.

MATERIALS AND METHODS

The cells used in this study, named All-15 cells, are a clonal isolate of mouse fibroblast NIH3T3 cells in which the four *Torpedo californica* AChR subunit cDNAs are stably integrated into the host genome. The four cDNAs were engineered into pSV2 expression plasmids and cotransfected with a neomycin-resistance selectable marker gene (pSV2-neo) using a calcium phosphate DNA-mediated gene transfer method (Claudio et al., 1987; Sine and Claudio, manuscript in preparation). All-15 cells were maintained in Dulbecco's modified Eagle's medium supplemented with 10% calf serum and 0.6 mg/ml geneticin (G418; Gibco Laboratories, Grand Island, NY) in a humidified atmosphere at 37°C with 5% CO_2. To induce expression of AChRs the medium was supplemented with 10 mM sodium butyrate and the cells were switched to a second incubator maintained at 24–26°C (Claudio et al., 1987). Currents were recorded from cells after 4–8 d at 24–26°C.

Single channel currents were recorded using standard patch clamp techniques (Hamill et al., 1981). The outside-out patch configuration was used for pilot experiments, but cell-attached recordings were used for all the data presented. The channels seen in the cell-attached configuration had the same general kinetic properties as those elicited by the application of ACh to outside-out patches. The temperature was 12 or 22 ± 1°C as specified. For all experiments cells were bathed in the following solution (in mM): 145 KCl, 1 $CaCl_2$, and 25 mM HEPES adjusted to pH 7.4 with 10–11 mM NaOH. The high potassium concentration was used to depolarize the cell to 0 mV so the membrane potential could be taken as minus the potential applied to the patch pipette. The "Ca^{2+}-free" pipette solution contained (in mM): 80 KF, 20 KCl, 40 potassium aspartate, 2 $MgCl_2$, 1 EGTA, and 10 HEPES adjusted to pH 7.4 with KOH. The "plus-Ca^{2+}" solution contained (in mM): 140 KCl, 0.5 $CaCl_2$, 0.5 $MgCl_2$, and 10 HEPES adjusted to pH 7.4 with KOH. ACh chloride (Sigma Chemical Co., St. Louis, MO) was kept frozen as 1 M aqueous stock solutions from which experimental pipette solutions were made fresh daily. Patch pipettes were fabricated from 7040 glass, obtained from Garner Glass Co., Claremont, CA. To obtain low noise recordings (rms readings of 145–170 fA at 3 kHz on our EPC-7 patch clamp), pipettes were coated with two or three coats

of Sylgard (Dow Corning Corp., Midland, MI) and the bath solution in contact with the pipette was minimized.

Single channel currents were recorded (EPC-7; List Electronic, Darmstadt, FRG), filtered (20 kHz, −3 db, 8-pole bessel), and sampled at 94 kHz using a pulse code modulator (model VR-10; Instrutech Corp., Mineola, NY) and a video cassette recorder. The digitized data were later transferred to an Atari 1040 ST computer at the 94-kHz sampling frequency using the VCATCH program. Like the program CATCH described by Sigworth (1983), VCATCH detects events and stores the relevant portions of the digital data stream from the VR-10, along with the information required to compute intervening closed intervals. It uses an improved event-detection algorithm in which a running average is computed at each sample point (averaging width two or four samples) and compared with symmetrical thresholds (±5 standard deviations of running-averaged background noise, typically ±2.5 pA) with respect to a local baseline estimate (average of 32 points).

Determination of open and closed times was done with the TAC program (based on THAC, described by Sigworth, 1983), which digitally filters the data (Gaussian response; final effective −3-db bandwidths were 10–20 kHz), interpolates with a cubic spline, and searches semiautomatically for transitions passing half the open channel current amplitude. The program estimates the times of threshold crossings by interpolation, and pulse durations so measured are corrected for the filter response to estimate actual dwell times (Eq. 17; Colquhoun and Sigworth, 1983). Errors in these estimates due to background noise on threshold-crossing times are expected to be small since the noise standard deviation was always less than 1/5 of the threshold (compare Figs. 11 and 12 of Colquhoun and Sigworth, 1983, in which the ratio was 1/4). Open- and closed-duration histograms were binned and displayed using a logarithmic time axis and a square root ordinate (Sigworth and Sine, 1987).

Typically a successful patch was stable for 5–10 min, had >1,000 opening transitions, and was free of non-AChR channels. In the best circumstances such recordings could be obtained ~50% of the time. The main factor determining the high level of activity was the temperature at which the cells were maintained while AChR expression was induced by sodium butyrate; cells maintained at 24°C as opposed to 26°C showed a substantially greater incidence of AChR channels (see Paulson and Claudio, 1989). Recordings made at 22°C always showed greater channel activity than those at 12°C.

Channels were sometimes observed that showed kinetic and conductance properties strikingly different from those associated with AChR activity. In outside-out patch experiments such channels never appeared in response to application of ACh. These channels were seen in cells not transfected with the *Torpedo* AChR genes, and in All-15 cells before AChR induction (which express no α-bungarotoxin binding sites). Recordings from patches showing appreciable activity of non-AChR channels were not analyzed.

Duration histograms were fitted in three stages. In the first stage both open- and closed-duration histograms were fitted to sums of exponentials using the binned maximum likelihood method (Sigworth and Sine, 1987), while a simplex search was used to vary the parameters (Caceci and Cacheris, 1984). From the fitted time constants, relative areas, and the histogram dead time, initial estimates were made of the probability of missing an opening or a closing and their mean durations (Blatz and Magleby, 1986). In the second stage these means and probabilities were put into our missed event correction routine, which fit the histograms to sums of exponentials (see Appendix I). This second stage fitting was repeated three times on each histogram, each time updating the mean durations and probabilities of missed events, to yield time constants and relative areas corrected for missed events. In the third stage of fitting the closed-duration histogram was fitted by varying rate constants in the four-state linear scheme plus channel block (Scheme 2, see below). Starting with a given set of scheme rate constants the set of areas and decay rates were obtained by numerically solving a cubic

equation (Colquhoun and Hawkes, 1981, Eqs. 3.65–3.67). These exponential parameters were then used together with the probability of missed openings (obtained in the second stage fitting) and the missed event correction procedure to yield a closed-time distribution corrected for missed events. The binned log likelihood was calculated from this distribution and the experimental histogram, and best-fit rate constants were found by repeating this process using the simplex search to maximize the log likelihood.

This rate constant fitting scheme (see also Blatz and Magleby, 1986) has several advantages over other methods of estimating rate constants from single-channel dwell time histograms. Instead of fitting major components to exponentials, correcting them for missed events after fitting, and then studying their concentration dependence, the entire closed-duration histogram is fitted by exponentials predicted by the scheme rate constants. This way even components predicted to have small areas are accounted for. Furthermore, by building the missed event correction into the fitting routine, the histograms are fitted by corrected exponentials.

The missed event correction is expected to be less reliable when both open and closed times approach the dead time (10–12 μs), as we find with ACh concentrations >100 μM; at this concentration the mean open duration is ~60 μs and the shortest closed-duration component has a mean of ~20 μs. Therefore, to independently verify the histogram fitting and also to extend time resolution, power spectra were computed from clusters of channel activity. Starting with raw data filtered at 20 kHz (bessel filter, −3 db) and digitized at 94 kHz, nonoverlapping stretches of $N = 256$–4,096 sample points (2.7–44 ms of data) were selected to contain either receptor-active or baseline intervals. After subtraction of the mean value, the data points for $t = 0$ to $N - 1$ were multiplied point-by-point by the window function,

$$w(t) = \begin{cases} \frac{1}{2}\left[1 - \cos\left(\frac{\pi/t}{w}\right)\right], & 0 \le t < w \\ 1, & w \le t < N - w \\ \frac{1}{2}\left[1 - \cos\left(\frac{\pi(N-t)}{w}\right)\right], & N - w \le t < N, \end{cases}$$

where the cosine-tapering width w was equal to 32 points in all cases. From the windowed data power spectra were computed by FFT, averages of 200–1,000 spectra were accumulated, and the baseline spectrum was subtracted to yield the spectrum due to channel activity.

At this point the high frequency points in the spectrum are attenuated due to the response of the recording system, which includes the 20-kHz bessel filter and the 37-kHz filter in the VR-10. Instead of measuring the impulse response of the system for computing a correction (Sigworth, 1985) we divided the channel-noise spectrum by a normalized resistor-noise spectrum obtained by connecting a 30-MΩ resistor to the patch clamp input as a source of "white" current noise. This correction removes the effect of the filtering on the spectrum by boosting the high frequencies. Edge effects due to unequal data values at the ends of the data window would give large high frequency artifacts under these conditions, which is the reason for using the tapered window described above. The resistor value was chosen according to the following considerations. High value resistors (≥1 GΩ) can yield distorted spectra because of nonuniformly distributed capacitance; low value resistors (≤3 MΩ) can introduce errors as they convert noise in the voltage command into current, as well as possibly reducing the bandwidth of the head-stage amplifier by excessively loading its input. We obtained spectra with the expected spectral density ($S = 4\ kT/R$) and identical high frequency rolloffs for resistors of $R = 3$–100 MΩ, indicating that a large range of values yields spectra free from the errors mentioned. To avoid contamination from noise in the command voltage we connected the resistor between the V_{ref} connector and the input terminal of the EPC-7 headstage; to

block possible dc currents due to the offset voltage of the headstage amplifier we inserted a 0.01-μF capacitor in series with the resistor.

For each recording both open- and closed-duration histograms were examined for stationarity. Each recording was divided into segments with equal numbers of events, typically four segments, and duration histograms were constructed. The histograms were fitted to the sum of exponentials, and the component parameters of each segment were compared with those of the other segments and those of the overall histogram. In addition, each segment histogram was superimposed over the others and the bin heights were compared to see whether they fell within the range of scatter defined by the square root–log duration histogram plot (see Sigworth and Sine, 1987, and text figures). Out of 56 records, 4 were excluded because they were nonstationary.

RESULTS

Experiments with Low ACh Concentrations

Fig. 1 illustrates single channel currents activated by low concentrations of ACh (0.5–1 μM) at 22°C, together with the corresponding open- and closed-duration histograms. The upper panel shows currents recorded without calcium in the recording pipette and the lower panel shows currents in the presence of calcium. In both sets of records currents appear either as isolated openings or as bursts of one or more openings separated by closed periods of tens of microseconds. Open-duration histograms (*left*) are well described by a single exponential distribution. A single exponential was always observed in the open-duration histograms obtained for 22°C experiments, but for experiments carried out at 12°C a small population of brief openings could be seen (open-duration fits for 0.5 μM ACh: $\tau_0 = 0.15$ ms, relative area = 0.12, $\tau_1 = 0.95$ ms, relative area = 0.88). The closed-duration histograms are described as the sum of two exponentials: a slow component (~100 ms) associated with periods between separate activation episodes, and a fast component (~10 μs) associated with multiple openings of a single ion channel (Colquhoun and Sakmann, 1985; Sine and Steinbach, 1986). The closed-duration histograms also show that brief channel closures, seen as the left-hand peaks, occur roughly twice as often when calcium is present in the recording pipette. As described below, this difference can be ascribed to differences in rate constants in a receptor activation scheme. Two components were always sufficient to fit the closed-duration histograms at low ACh concentrations; additional components of intermediate duration were never seen.

The low concentration measurements were interpreted according to the following four-state activation scheme:

$$2A + R \underset{k_{-1}}{\overset{k_{+1}}{\rightleftharpoons}} AR + A \underset{k_{-2}}{\overset{k_{+2}}{\rightleftharpoons}} A_2R \underset{\alpha}{\overset{\beta}{\rightleftharpoons}} A_2R^*$$

Scheme 1

In Scheme 1 the agonist A binds to the receptor R with rate constants k_{+1} and k_{+2}, and dissociates with rates k_{-1} and k_{-2}. Fully occupied receptors A_2R open with rate β and active receptors A_2R^* close with rate α. Because only one component of brief closures is seen at low ACh concentrations, it can be associated with dwells in the

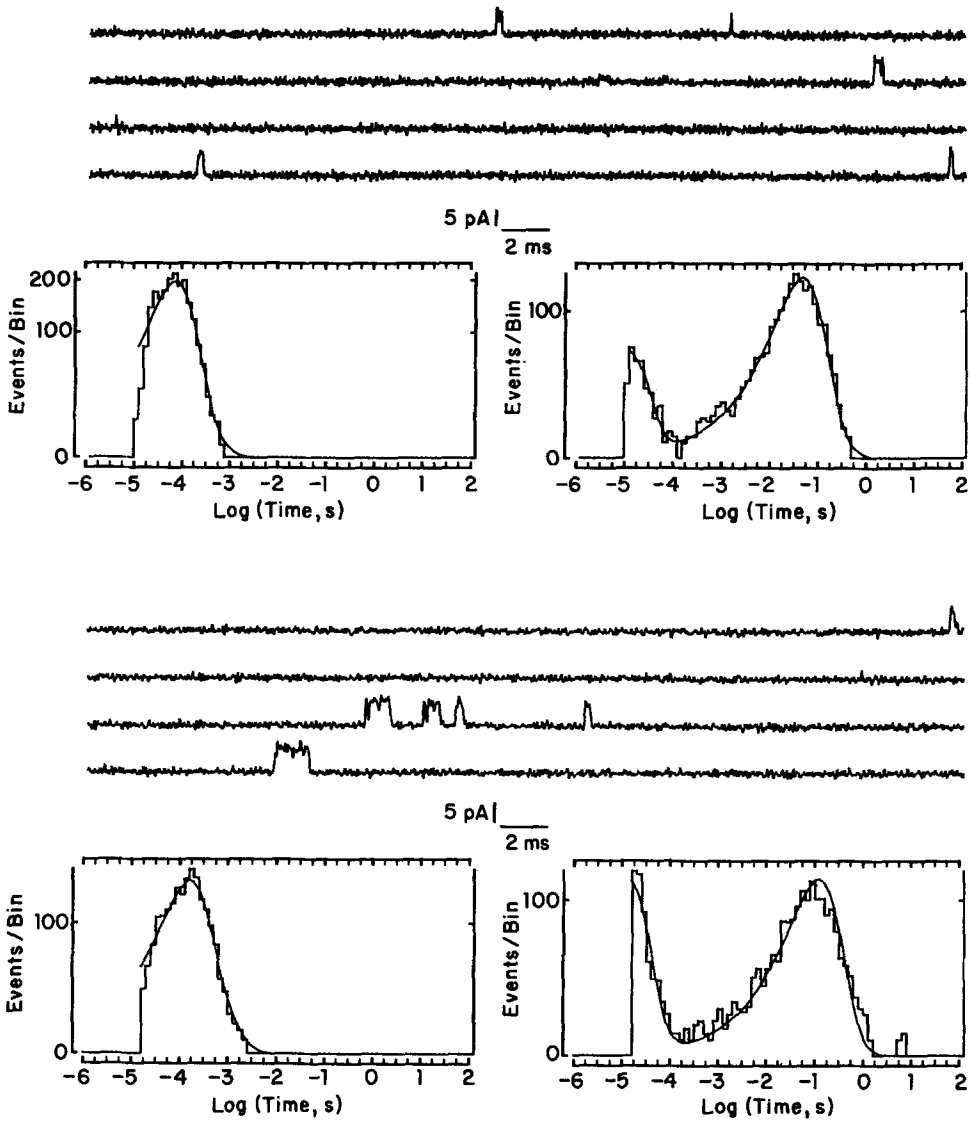

FIGURE 1. Single channel currents (upward deflections) and corresponding open- (*left*) and closed-duration (*right*) histograms recorded at 22°C at −70 mV in the presence of 1 μM ACh, Ca^{2+}-free (*top*) or in the presence of 0.5 μM ACh plus Ca^{2+} (*bottom*). Continuous segments are shown low-pass filtered at 15 kHz (*top record*) or 12 kHz (*bottom record*). For both records the open-duration histogram is fitted by a single exponential, and the closed-duration histogram by the sum of two exponentials (all corrected for missed events). For plotting these and subsequent histograms we used a square root ordinate and a logarithmic abscissa. For the Ca^{2+}-free histograms (*top*) the fitted parameters are: for open durations, $\tau_0 = 69.8$ μs and total events $n = 2{,}680$; for closed durations, $\tau_0 = 10.8$ μs, $a_0 = 0.279$, $\tau_1 = 48.4$ ms, $a_1 = 0.721$, $n = 2{,}670$. For the plus-Ca^{2+} recordings (*bottom*) the fitted parameters are: for open durations, $\tau_0 = 144$ μs, $n = 2{,}790$; for closed durations, $\tau_0 = 11.9$ μs, $a_0 = 0.518$, $\tau_1 = 0.119$ s, $a_1 = 0.482$, $n = 3{,}190$. Note the increased number of brief closings in the presence of calcium.

A_2R closed state. At limiting low concentrations these closures are predicted to have a time constant of $(\beta + k_{-2})^{-1}$ and to occur at β/k_{-2} closures per burst of openings (Colquhoun and Hawkes, 1981). The number of brief closures was computed as the total area of the brief component. The number of bursts was found by first defining a burst as a series of openings separated by closures shorter than a defined critical time (here 100 μs), and then computing the number of bursts as the area of the fitted burst duration histogram (Sine and Steinbach, 1986).

The low concentration measurements were made using 0.5–1 μM ACh because channel events became too rare at lower concentrations. Since these concentrations are not vanishingly small, the agonist has a finite probability of rebinding after dissociating. However, the analysis described below demonstrates that the time constant and area of the brief closed-duration component exhibit little change up to 100 μM ACh, and that the probability of rebinding within 100 μs is $<10^{-3}$ at 1 μM ACh. Further, although 0.5–1 μM ACh is sufficient to desensitize ~50% of the receptors at steady state (Sine and Claudio, manuscript in preparation), closures due to desensitization are so long that they can be readily distinguished from brief closures due to activation processes.

If the two ACh binding sites are identical, the rate constants k_{+1} and k_{-2} in Scheme 1 should be interpreted as macroscopic constants, which should be statistically weighted (i.e., divided by two) to obtain the microscopic rate constants. However, if the affinities for the two sites are very different (i.e., $k_{-1}/k_{+1} \ll k_{-2}/k_{+2}$ as we demonstrate below), k_{+1} and k_{-2} correspond directly to the microscopic rate constants.

Table I summarizes both the measured parameters and the computed rate constants for the low concentration experiments. At 22°C and in the absence of external calcium the channel opening rate β is 22,000 s^{-1}. External calcium increases β about twofold, consistent with the more burst-like openings seen in Fig. 1. Ca^{2+} might be expected to affect gating kinetics, since it is well known to increase the affinity of cholinergic agonists (Cohen et al., 1974; see below). However, in our experiments we cannot exclude the possibility that the different anions in the Ca^{2+}-free and the plus-Ca^{2+} solutions contribute to the kinetic changes. Decreasing the temperature from 22 to 12°C slows β about fourfold. At 22°C and in the absence of calcium the rate of ACh dissociation k_{-2} is 70,000 s^{-1}. In the presence of calcium, k_{-2} decreases in magnitude to become comparable to β, so the probability that a channel reopens increases to ~0.5. The 10°C decrease in temperature slows k_{-2} threefold. The channel closing rate α, the slowest of the three rates, slows from 15,000 to 8,000 s^{-1} in the presence of Ca^{2+}, and from 15,000 to 1,000 s^{-1} between 22 and 12°C.

One patch, recorded at 22°C and in the absence of external calcium, was stable enough to study low concentration kinetic parameters over a range of membrane voltages (Fig. 2). The mean duration of brief closures exhibits no voltage dependence, whereas the number of closures per burst decreases at more negative voltages (e-fold per 137 mV) and the mean burst duration increases (e-fold per 163 mV). The number of closures per second of open time thus shows greater voltage dependence (e-fold per 69 mV) than either closures per burst or burst duration. The computed

rate constants are thus weakly voltage dependent; both β and α decrease at negative voltages (*e*-fold per 141 and 155 mV, respectively), whereas k_{-2} shows no voltage dependence.

In the presence of calcium a somewhat different voltage dependence is seen. Although examined only at -70 and -100 mV, β appears to increase at more negative voltages, whereas k_{-2} and α show no voltage dependence (Table I).

The single channel conductance, measured from current amplitudes at -70 mV, is 119 pS in the Ca^{2+}-free external solution and 91 pS in the plus-Ca^{2+} solution. Somewhat lower than physiological concentrations of divalent ions were used because at higher calcium concentrations the currents become too small to be resolved at 10 kHz bandwidth (see Imoto et al., 1986).

TABLE I

Low Concentration Closed-duration Parameters and Derived Rate Constants

Conditions	*n*	τ_{open}	τ_{burst}	$1/\tau_{fast}$	gaps/burst	gaps/s	beta	k_{-2}	alpha
		μs	μs	s^{-1}			s^{-1}	s^{-1}	s^{-1}
22°C	3	73.9	84.8	100,600	0.359	4,300	26,600	74,000	15,200
$-Ca^{2+}$, -70 mV		(5.0)	(5.3)	(7,030)	(0.013)	(380)	(2,500)	(4,500)	(960)
1–2 μM ACh									
22°C	4	169	228	85,607	1.09	4,900	44,700	40,900	8,400
$+Ca^{2+}$, -70 mV		(32)	(39)	(4,100)	(0.06)	(1,004)	(2,200)	(2,000)	(2,200)
0.5–2 μM ACh									
22°C	3	151	246	100,200	1.59	6,500	61,450	38,700	8,700
$+Ca^{2+}$, -100 mV		(3.5)	(11)	(3,700)	(0.03)	(380)	(2,700)	(1,000)	(320)
0.5–2 μM ACh									
12°C	1	867	1,100	27,500	0.218	220	4,900	22,600	1,200
$+Ca^{2+}$, -100 mV									
0.5 μM ACh									
12°C	2	1,220	1,580	24,900	0.314	210	5,700	19,100	900
$-Ca^{2+}$, -100 mV		(41)	(219)	(10,500)	(0.060)	(58)	(1,600)	(8,900)	(22)
2 μM ACh									

For the specified recording condition mean values of closed-duration parameters are presented. The values in parentheses are the standard deviations for *n* experiments.

The low concentration experiments can be summarized as follows. A single brief closed time component is observed, which we associate with dwells in the ACh_2R state (see Scheme 1). Analysis of this brief component allows estimation of β, k_{-2}, and α. The ratio β/α, although favoring the open state, is only 5.3 and 1.8 for plus and minus calcium, respectively. Extracellular calcium appears to increase the efficiency of the receptor by increasing β and decreasing k_{-2} and α. The apparent Q_{10}'s seem reasonable for k_{-2} (3-fold) and β (4-fold), but are unusually high for α (15-fold). However, as will be shown below, the remaining Scheme 1 rates are even more temperature sensitive. Most important for the following analysis, β and k_{-2} are now known parameters. They can thus be held constant in fitting closed-duration histograms obtained at raised ACh concentrations.

Experiments with Raised ACh Concentrations

At ACh concentrations greater than 10 μM receptors activate in episodes of intense channel activity, called clusters, separated by prolonged intercluster closed periods. Fig. 3 shows a single cluster elicited by 100 μM ACh. Also shown are the corresponding open- and closed-duration histograms. The cluster consists of several

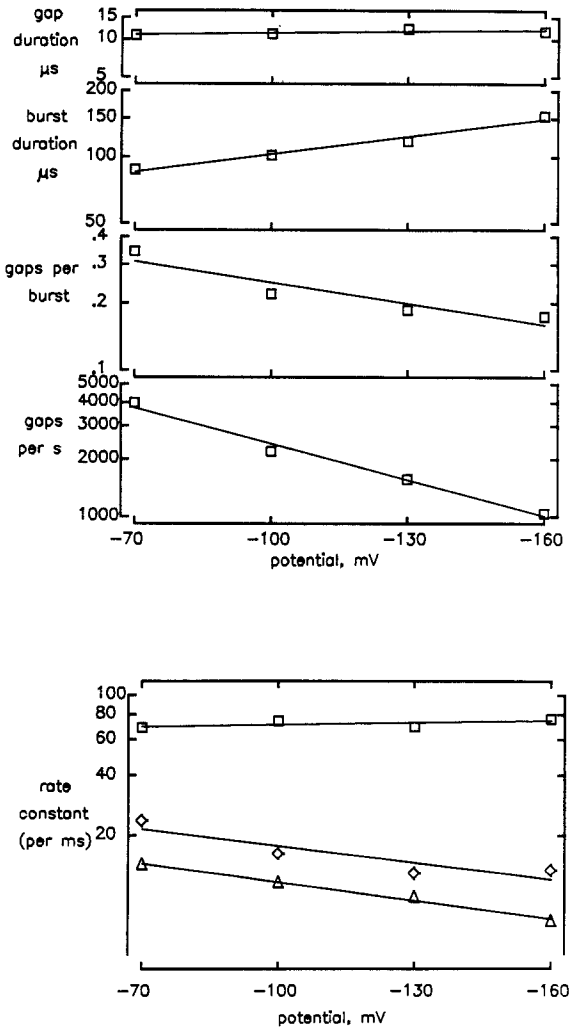

FIGURE 2. Voltage dependence of parameters for currents elicited by 1 μM ACh at 22°C, Ca^{2+}-free. The straight lines are least-squares fits. First panel, Mean duration of brief closures; *e*-fold increase per 949 mV. Second panel, Mean burst duration; *e*-fold increase per 163 mV. Third panel, Number of brief closures per burst of openings; *e*-fold decrease per 137 mV. Fourth panel, Number of brief closures per second of open time; *e*-fold decrease per 68.9 mV. Fifth panel, Voltage dependence of Scheme 1 transition rates; k_{-2}, *e*-fold increase per 1,255 mV; β, *e*-fold decrease per 155 mV; and α, *e*-fold decrease per 141 mV.

groups of closely spaced openings separated by intracluster closures of several milliseconds. This clustering and grouping of openings is a pattern characteristic of raised agonist concentrations (Sakmann et al., 1980; Sine and Steinbach, 1984, 1987; Auerbach and Lingle, 1987). We interpret the long closures between clusters as resulting from the slow recovery of desensitized receptors; they are visible in the

closed-duration histogram as the component at the far right which has a small area and a time constant of ~5 s. Similarly, the long closures within the cluster are taken to represent the recovery of a single receptor from a more rapidly recovering desensitized state; these intergroup closures contribute the second small component, which has a mean of ~30 ms. We assume that intergroup closures separate activation episodes whose activity is represented in Scheme 1. Closures due to activation processes, which here are fitted by the sum of two exponentials, are easily distinguished from the longer and less frequent intergroup closures. Activation closures are defined as those shorter than a specified critical time, which is taken as the time

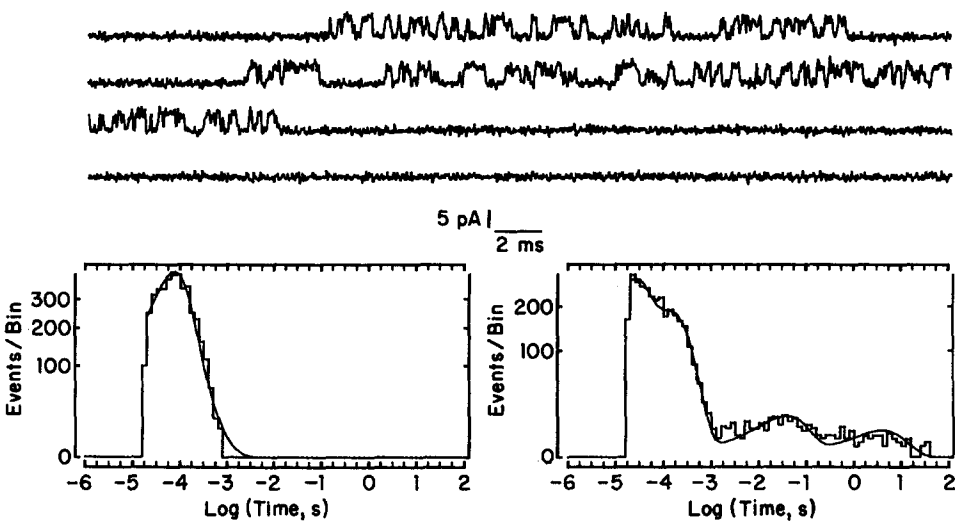

FIGURE 3. Cluster of channel openings elicited by 100 μM ACh at 22°C plus-Ca^{2+}, and the corresponding open- and closed-duration histograms. A continuous segment of record is shown filtered at 12 kHz. A single cluster is displayed which consists of several groups of closely spaced openings separated by closures longer than 2 ms. The open-duration histogram (*left*) is fitted by a single exponential, whereas the closed-duration histogram (*right*) is fitted by the sum of four exponentials. The fitted parameters are: open durations, τ_0 = 65.2 μs, n = 8,880; closed durations, τ_0 = 16.4 μs, a_0 = 0.54, τ_1 = 135 μs, a_1 = 0.42, τ_2 = 28 ms, a_2 = 0.03, τ_3 = 3.4 s, a_3 = 0.01, n = 9,250.

at which the exponential fitted to the slowest activation component intersects that fitted to the fast desensitization component.

The 100-μM open-duration histogram exhibits a shorter mean duration (65 μs) than is seen at low ACh concentrations (141 μs, Fig. 1). The shorter duration is an expected consequence of open channel block by ACh. As described further below, these blockages are brief (tens of microseconds), their duration does not change with ACh concentration, and their frequency increases in proportion to the ACh concentration. To account for channel block at high ACh concentrations the following expanded scheme was used in fitting the activation portion of the

closed-duration histograms:

$$2A + R \underset{k_{-1}}{\overset{k_{+1}}{\rightleftharpoons}} AR + A \underset{k_{-2}}{\overset{k_{+2}}{\rightleftharpoons}} A_2R \underset{\alpha}{\overset{\beta}{\rightleftharpoons}} A_2R^* + A \underset{k_{-b}}{\overset{k_{+b}}{\rightleftharpoons}} A_2R_{blocked}$$

Scheme 2

In Scheme 2, the agonist A reversibly blocks open channels with the forward rate constant, k_{+b}, and unblocks with rate k_{-b}. The block illustrated in Scheme 2 is a classical local anesthetic type block (Neher and Steinbach, 1978), which has also been used to describe agonist block of other AChR channels (Sine and Steinbach, 1984; Ogden and Colquhoun, 1985). For Scheme 2 the closed-duration histogram is described by a probability density function (pdf) obtained by differentiating the following probability distribution function:

$$F(t) = 1 - (1 - f_b)[a_0 \exp(-\lambda_0 t) + a_1 \exp(-\lambda_1 t) + a_2 \exp(-\lambda_2 t)] - f_b \exp(-k_{-b} t), \quad (1)$$

where the fraction of closures due to channel block f_b equals $k_{+b}[ACh]/(k_{+b}[ACh] + \alpha)$, and k_{-b} is the unblocking rate constant. The a_n and λ_n are relative areas and decay rates for the activation portion of Scheme 2 (steps to the left of A_2R^*). The λ_n's are determined by the rate constants of Scheme 2, and are roots of a cubic equation (see Colquhoun and Hawkes, 1981, and Methods).

In the limit of low ACh concentrations the three activation components of Eq. 1 can be identified with particular state transitions in Scheme 2 as follows. One exponential term arises from channels that close and reopen without losing bound ACh; its rate λ_0 equals $\beta + k_{-2}$, as described earlier. A second term arises from channels that close and lose only one ACh before reopening; its rate λ_1 approaches k_{-1}, the rate of leaving the AR state. The third term arises from channels that close and lose both ACh molecules before reopening; at limiting low concentrations its rate λ_2 increases with the square of the ACh concentration. At higher concentrations the components cannot be strictly associated with individual state transitions, although it is important to note that the third term predominates at saturating concentrations, where its rate λ_2 approaches β.

In the histograms the two slowest closed-duration components are assumed to arise from fast and slow desensitization. Therefore, in the following analysis of intermediate and high concentration data these components were fitted as the sum of exponentials, and their contribution was subtracted from the portion of the histogram shorter than the critical time. The pdf for Scheme 2 was then fitted only to histogram bins shorter than the critical time (Sine and Steinbach, 1987). Errors due to this subtraction procedure are expected to be small because the desensitization components are small and well separated from the activation components. In the following figures we show the original unsubtracted histograms, with the fitted pdf and the two "desensitization" components superimposed.

Experiments with Intermediate ACh Concentrations

In fitting the closed-duration histograms obtained at intermediate ACh concentrations (10–30 μM) β and k_{-2} were fixed to the values measured at low ACh concentrations, and as an initial approximation k_{-1} was constrained to be $k_{-2}/2$. The unblocking rate k_{-b} was also a fixed parameter, as it was estimated from histogram analysis of recordings at high concentrations as described below. The histograms were therefore fitted by varying k_{+1}, k_{+2} and f_b. Fig. 4 shows the best fit, given the set of fixed rates. The fit fails to describe the excess closures near the trough at 100 μs, and overshoots the the major peak of closures at 2 ms. The major peak of closed times is therefore wider than predicted for a single exponential centered in that region. This disparity between the Scheme 2 fit and the data was very reproducible; it was seen for each of the three sets of recording conditions at intermediate ACh concentrations (two or three patches per condition), and in each histogram constructed from four equal segments of a single record. This consistently poor fit led us to suspect that k_{-1} might not simply equal $k_{-2}/2$. In addition, using the assumed k_{-1}, the fitted k_{+1} was always $\sim 1 \times 10^9$ $M^{-1}s^{-1}$, a value somewhat greater than diffusion-limited.

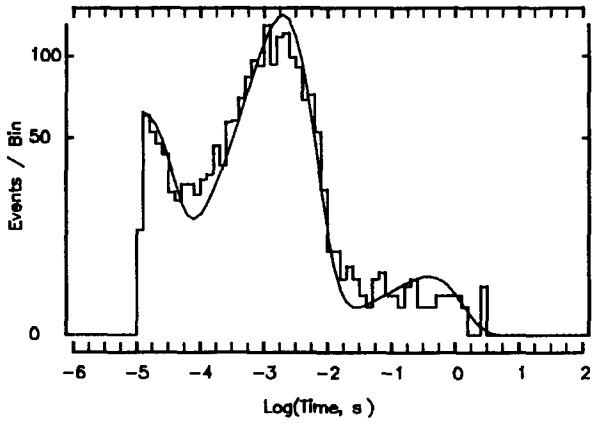

FIGURE 4. Closed-duration histogram obtained with 30 μM ACh, Ca^{2+}-free at 22°C, and fitted by Scheme 2 with k_{-1} set at $k_{-2}/2$. Scheme 2 is fitted to the activation portion of the histogram (times less than 20 ms) with parameters fixed as follows: β = 22,000 s^{-1}, k_{-2} = 70,000 s^{-1}, and k_{-1} = 35,000 s^{-1}, k_{-b} = 80,000 s^{-1}. The fitted parameters are: k_{+1} = 1.28×10^9 $M^{-1}s^{-1}$, k_{+2} = 1.44×10^8 $M^{-1}s^{-1}$, f_b = 0.13, n = 2,556. Desensitization closures are fitted with a single exponential component with τ = 0.379 s^{-1} and n = 53. Note that the fit misses the excess events around 100 μs and the shortage around 2 ms.

To determine the dissociation rate k_{-1}, we assigned it different fixed values and varied the association rates so as to maximize the log likelihood as described above. The right panel in each part of Fig. 5 shows the maximum log likelihood plotted against the fixed k_{-1} value. The plots show a clear and statistically significant optimum value for each of the three recording conditions. Each left panel shows the corresponding closed-duration histogram with the superimposed best fit. The entire range of activation closed times is now well described by Scheme 2 and a unique value of k_{-1}; the fit also discloses unique values of k_{+1} and k_{+2}.

The assignment of k_{-1} is made possible by the broad envelope of closures centered

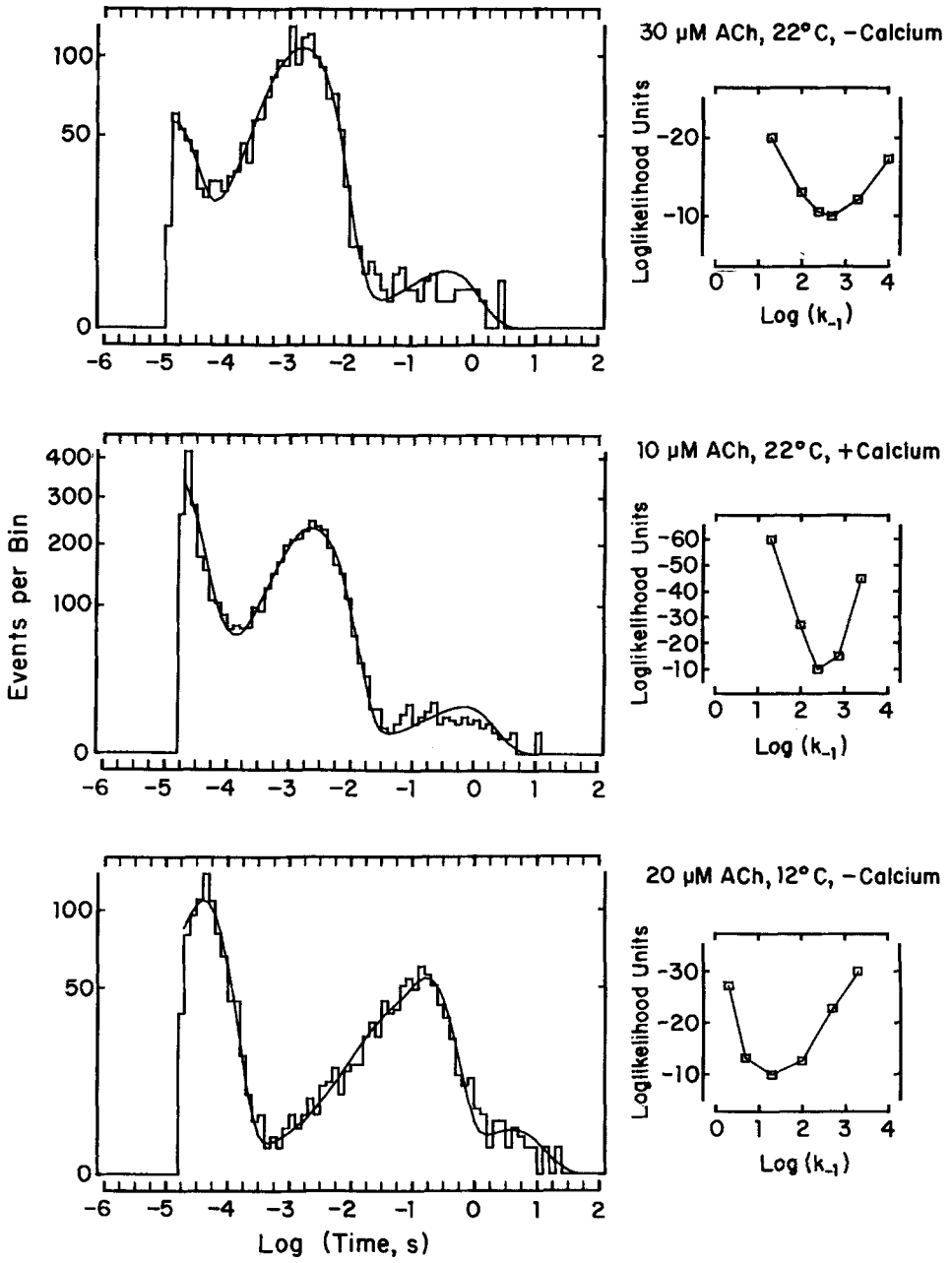

FIGURE 5. Determination of k_{-1}. In each of the three panels the log likelihood (relative values) is plotted against the value of k_{-1} held constant in fitting, and the closed-duration histogram analyzed is shown fitted with the optimum k_{-1} value. *Top*, 30 μM ACh, Ca^{2+}-free, 22°C (same as Fig. 4). Fixed parameters: β = 22,000 s^{-1}, k_{-2} = 70,000 s^{-1}, k_{-1} = 500 s^{-1}, k_{-b} = 70,000 s^{-1}. Fitted parameters: k_{+1} = 2.96 × 10^7 $M^{-1}s^{-1}$, k_{+2} = 1.14 × 10^8 $M^{-1}s^{-1}$, f_b = 0.117, n = 2,510. *Middle*, 10 μM ACh, plus-Ca^{2+}, 22°C. Fixed parameters: β = 45,000 s^{-1}, k_{-2} = 40,000 s^{-1}, k_{-1} = 250 s^{-1}, k_{-b} = 35,000 s^{-1}. Fitted parameters: k_{+1} = 6.02 × 10^7 $M^{-1}s^{-1}$, k_{+2} = 9.82 × 10^7 $M^{-1}s^{-1}$, f_b = 0.133, n = 8,540. Desensitization component fitted with τ = 0.661 s, n = 121. *Bottom*, 20 μM ACh, Ca^{2+}-free, 12°C. Fixed parameters: β = 5,000 s^{-1}, k_{-2} = 20,000 s^{-1}, k_{-1} = 20 s^{-1}, k_{-b} = 24,000 s^{-1}. Fitted parameters: k_{+1} = 1.01 × 10^6 $M^{-1}s^{-1}$, k_{+2} = 3.52 × 10^6 $M^{-1}s^{-1}$, f_b = 0.52, n = 2,130. Desensitization component fitted with: τ = 4.0 s, n = 34. For each of the three recording conditions a clear optimum k_{-1} is obtained which allows the activation portion of each histogram to be described by Scheme 2. A log likelihood difference of 2 is significantly different to the 1% confidence level (Colquhoun and Sigworth, 1983).

at ~2 ms for the 22°C experiments and at ~100 ms for the 12°C experiments. For the 22°C experiments this envelope consists of two closely spaced components (time constants ~2 ms and 0.5 ms for the Ca^{2+}-free experiments) with similar relative areas (~0.5 and 0.2). Although it would be difficult to uniquely fit this envelope to the sum of exponentials, the constraints imposed by the scheme rate constants allow us to obtain a unique fit and good precision in estimating the rate constants. For the 12°C experiments the two components are more clearly separated, with time constants of 170 and 20 ms.

TABLE II

Summary of Fitted Scheme 2 Rate Constants

Conditions	n	k_{+1}	k_{+2}	k_{+b}
			$(M^{-1}s^{-1})$	
22°C, $-Ca^{2+}$:				
10 μM, −70 mV	3	$6.1 \pm 0.2 \times 10^7$	$4.3 \pm 1.0 \times 10^7$	$1.4 \pm 0.1 \times 10^8$
30 μM, −70 mV	4	$4.6 \pm 1.9 \times 10^7$	$8.7 \pm 1.7 \times 10^7$	$7.9 \pm 2.2 \times 10^7$
30 μM, −100 mV	2	5.2×10^7	$9.2 \pm 0.9 \times 10^7$	$9.0 \pm 0.6 \times 10^7$
100 μM, −70 mV	4	$6.5 \pm 0.5 \times 10^7$	$1.1 \pm 0.1 \times 10^8$	$4.0 \pm 0.8 \times 10^7$
300 μM, −70 mV	4	$5.9 \pm 1.2 \times 10^7$	$1.1 \pm 0.3 \times 10^8$	$3.7 \pm 0.9 \times 10^7$
22°C, $+Ca^{2+}$:				
10 μM, −70 mV	2	$5.8 \pm 0.5 \times 10^7$	$8.4 \pm 0.3 \times 10^7$	$9.2 \pm 0.9 \times 10^7$
10 μM, −100 mV	1	6.3×10^7	9.9×10^7	2.7×10^8
30 μM, −70 mV	4	$6.2 \pm 0.5 \times 10^7$	$8.8 \pm 1.6 \times 10^7$	$5.5 \pm 1.1 \times 10^7$
30 μM, −100 mV	3	$5.9 \pm 2.3 \times 10^7$	$8.1 \pm 1.6 \times 10^7$	$7.3 \pm 1.8 \times 10^7$
100 μM, −70 mV	4	$6.2 \pm 1.1 \times 10^7$	$1.3 \pm 0.2 \times 10^8$	$4.3 \pm 0.7 \times 10^7$
100 μM, −100 mV	2	$6.6 \pm 0.7 \times 10^7$	$1.3 \pm 0.1 \times 10^8$	$4.6 \pm 0.4 \times 10^7$
300 μM, −70 mV	1	5.6×10^7	1.3×10^8	3.5×10^7
12°C, $-Ca^{2+}$:				
10 μM, −100 mV	2	$1.5 \pm 0.2 \times 10^6$	$2.4 \pm 0.1 \times 10^6$	$4.8 \pm 0.7 \times 10^7$
20 μM, −100 mV	2	1.1×10^6	3.5×10^6	5.9×10^7
30 μM, −100 mV	2	1.1×10^6	$2.9 \pm 0.9 \times 10^6$	$4.7 \pm 0.3 \times 10^7$
100 μM, −100 mV	3	$1.0 \pm 0.1 \times 10^6$	$3.0 \pm 0.1 \times 10^6$	$4.3 \pm 0.4 \times 10^7$
300 μM, −100 mV	3	$1.0 \pm 0.1 \times 10^6$	$2.3 \pm 1.0 \times 10^6$	$3.0 \pm 0.5 \times 10^7$

The means of the fitted rates k_{+1} and k_{+2} (±SD) were determined for n experiments as described in the text. The following fixed rates were used in the analysis (all in s^{-1}): 22°C, Ca^{2+}-free: $\beta = 22{,}000$, $k_{-2} = 70{,}000$, $k_{-1} = 500$, $k_{-b} = 7{,}0000$ (−70 mV) or 50,000 (−100 mV); 22°C, plus-Ca^{2+}: $\beta = 4{,}5000$, $k_{-2} = 40{,}000$, $k_{-1} = 250$, $k_{-b} = 40{,}000$ (−70 mV) or 30,000 (−100 mV); 12°C, Ca^{2+}-free: $\beta = 5{,}000$, $k_{-2} = 20{,}000$, $k_{-1} = 20$, k_{-b} was fitted for each histogram as described in the text and Fig. 13. k_{+b} was determined using text Eqs. 2 and 3.

For the 22°C experiments k_{-1} is 500 s^{-1} in the Ca^{2+}-free solution and 250 s^{-1} in the plus-Ca^{2+} solution. For both ionic conditions k_{-1} is ~350 times slower than k_{-2}. The fitted association rates, 6×10^7 and 1×10^8 $M^{-1}s^{-1}$, approach diffusion limited values (Fig. 5 legend and Table II). Moreover, the dissociation constant for the first agonist binding site (4.2 μM for plus-Ca^{2+} and 8.3 μM for Ca^{2+}-free) is about two orders of magnitude lower than that for the second site (400 μM for plus-Ca^{2+} and 700 μM for Ca^{2+}-free). The primary sources of the affinity difference are the dissociation rates. Channel block, which contributes only a small fraction of closures here at intermediate concentrations, will be fully examined below.

At 12°C k_{-1} is 20 s^{-1}, ~25-fold lower than that estimated at 22°C. The singly occupied receptor is thus relatively stable at 12°C. Slowed even more by lowered temperature are the association rate constants: 1×10^6 and 3×10^6 M^{-1} s^{-1} for the first and second steps, respectively (Table II). These rates are 60- and 33-fold slower than the corresponding rates estimated at 22°C. As seen at 22°C, at 12°C the dissociation constants are different for the two sites (20 μM and 6.6 mM).

High Concentration Measurements

To test the rate constant estimates for consistency they were also examined across a range of high ACh concentrations. Fig. 6 exhibits currents recorded at several ACh concentrations at 22°C in Ca^{2+}-free solution, along with the companion closed-duration histograms and fitted Scheme 2 pdf's. The current traces show progressively tighter packing of openings as the ACh concentration increases. This tighter packing is also demonstrated in the closed-duration histograms where the major peak shifts from long durations (~20 ms at 10 μM ACh) to short durations (~200 μs at 300 μM ACh). The major peak, which is narrow at 10 μM, broadens at 30 μM and narrows again at 100 and 300 μM.

The fitted pdf's (smooth curves) were obtained by fitting the Scheme 2 rate constants to the data. As described for the intermediate concentration analysis, k_{+1} and k_{+2} were varied, while β and k_{-2} were fixed to the values determined from the low concentration measurements. The value of k_{-1} was fixed to that determined from the intermediate concentration measurements. f_b was also varied, whereas k_{-b} was again held constant to the value determined in the following section on channel block. The histograms are well described by Scheme 2. Moreover, the best fit rate constants used to construct the smooth curves are essentially the same as those just determined in fitting the intermediate concentration data (see legends to Figs. 5 and 6 and Table II).

To further illustrate the generality of the fitted rate constants, Fig. 7 shows the concentration dependence of each of the three decay rates λ_n and the corresponding amplitudes a_n from the fitted closed-duration distributions (Eq. 1). The curves were computed from the grand means of the rate constants obtained at 22°C without calcium (Table III). Individual points show the decay rates and amplitudes of the exponential components obtained by fitting the Scheme 2 predictions to the data, as in Fig. 6. The squares represent the parameters λ_0 and a_0 of the single brief closed-time component seen at low ACh concentrations, which we associate with dwells in the A_2R state; neither parameter changes appreciably until the ACh concentration exceeds 100 μM. Using 0.5–1 μM ACh as a limiting low concentration therefore seems to be a reasonable approximation. The triangles show the intermediate duration component λ_1, which is seen best at 10–30 μM ACh and is associated with the loss of one ACh before reopening; its rate λ_1 equals k_{-1} at limiting low concentrations and increases linearly with concentration, while its area a_1 peaks near the dissociation constant for the first binding site. The diamonds represent the slow component, which has the rate λ_2; it has been termed the "β'" component because it is the major concentration-dependent component whose rate approaches a limiting value of β. Since at low concentrations this component arises from loss and rebinding of two ACh molecules, its rate initially increases with the square of the

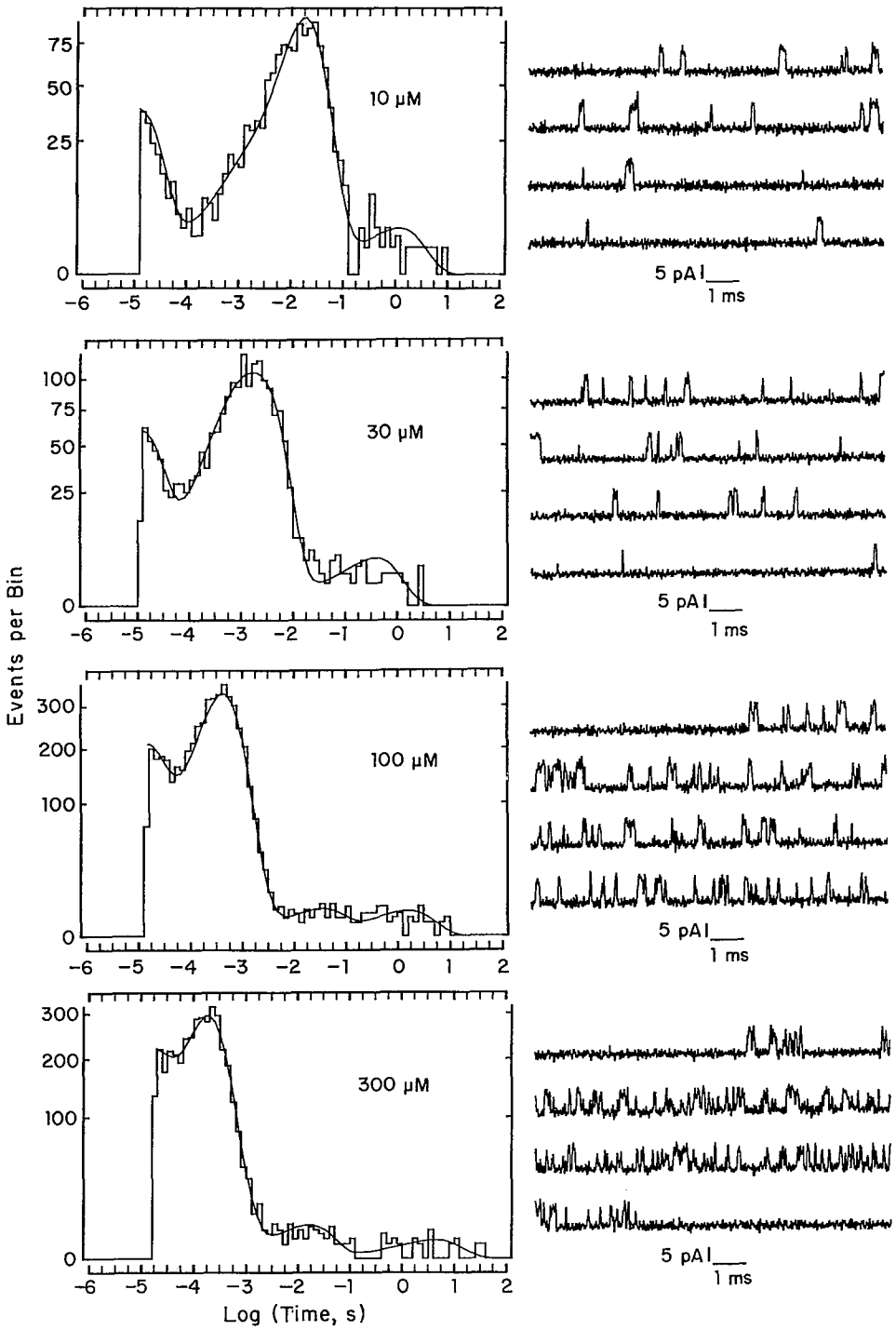

FIGURE 6. Concentration dependence of closed durations for currents recorded at 22°C Ca^{2+}-free. In each of the four panels a continuous record segment is shown beginning with the start of a cluster (12 kHz filtering). Alongside is the corresponding closed-duration histogram fitted to Scheme 2 as in Fig. 5. The fixed parameters, β, k_{-2}, k_{-1}, and k_{-b} are the same values used in Fig. 5, *top*. The fitted parameters are as follows. Top panel (10 μM ACh): $k_{+1} = 5.1 \times 10^7\ M^{-1}s^{-1}$, $k_{+2} = 5.0 \times 10^7\ M^{-1}s^{-1}$, $f_b = 0.084$, $n = 1{,}820$. Second panel (30 μM ACh): $k_{+1} = 2.96 \times 10^7\ M^{-1}s^{-1}$, $k_{+2} = 1.14 \times 10^8\ M^{-1}s^{-1}$, $f_b = 0.117$, $n = 2{,}510$. Third panel (100 μM ACh): $k_{+1} = 6.49 \times 10^7\ M^{-1}s^{-1}$, $k_{+2} = 1.20 \times 10^8\ M^{-1}s^{-1}$, $f_b = 0.23$, $n = 7{,}840$. Bottom panel (300 μM ACh): $k_{+1} = 6.04 \times 10^7\ M^{-1}s^{-1}$, $k_{+2} = 1.06 \times 10^8\ M^{-1}s^{-1}$, $f_b = 0.32$, $n = 7{,}780$. As the concentration of ACh increases the openings cluster more tightly and the major envelope of closed durations moves toward shorter time.

ACh concentration, but at higher concentrations its rate increases linearly with the concentration. The close correspondence between data and theory shows that a single set of rate constants describes the closed-time distributions over the entire range of ACh concentrations.

Fig. 8 exhibits currents and histograms obtained at 22°C with the plus-Ca^{2+} solution. Again, as the concentration of ACh increases, the current traces show progressively tighter packing of openings, and the histograms show a long- to short-duration shift of the major peak of closed durations. In contrast to the calcium-free recordings, the major closed-duration peak is broadest at 10 μM instead of 30 μM, owing to tighter binding of ACh to the first site in the presence of calcium (4.2 vs. 8.3 μM). Because the open durations are longer, block by ACh is more clearly

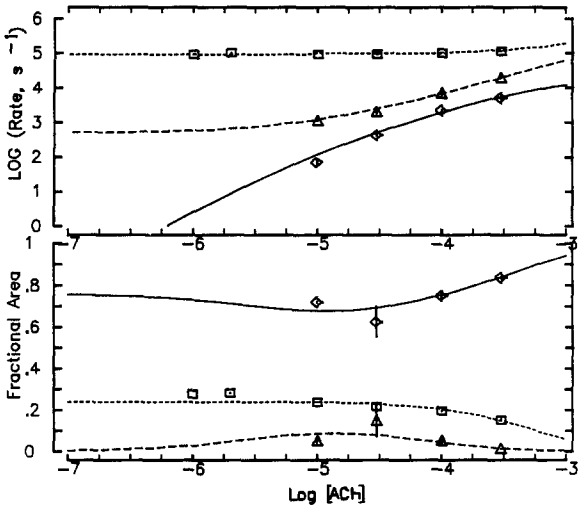

FIGURE 7. Concentration dependence of the rates (*top*) and areas (*bottom*) of the three activation components for the 22°C Ca^{2+}-free measurements. The curves are those predicted for the activation portion of Scheme 2 by the grand mean of fitted rate constants (Table II). The curves were computed by numerically solving the cubic equation given by Colquhoun and Hawkes (1981; see Eqs. 3.65–3.75). The symbols represent mean values ± the standard deviation for each component parameter corresponding to the Scheme 2 rate constants fitted to each histogram. The areas are expressed as the fraction of the total area of activation components. Only one set of symbols is shown for 1 and 2 μM ACh because only the rapid closed-time component for a single channel could be discerned at those low concentrations.

apparent, as seen at 300 μM ACh where the concentration-dependent activation components merge with the concentration-independent blocking component. Again the histograms are well described by Scheme 2 and essentially the same rate constants are determined at intermediate concentrations (Table II).

Fig. 9 displays the concentration dependencies of the decay rates and amplitudes computed from the fitted activation rate constants for the 22°C, plus-Ca^{2+} experiments. As seen for the calcium-free experiments, a single set of rate constants describes the components of the closed-duration histograms over a wide range of ACh concentrations. Again the A_2R closures seen at low concentrations (squares) change little until the ACh concentration exceeds 100 μM. The area, however, is about twice as great as in the absence of calcium, consistent with the increased β and

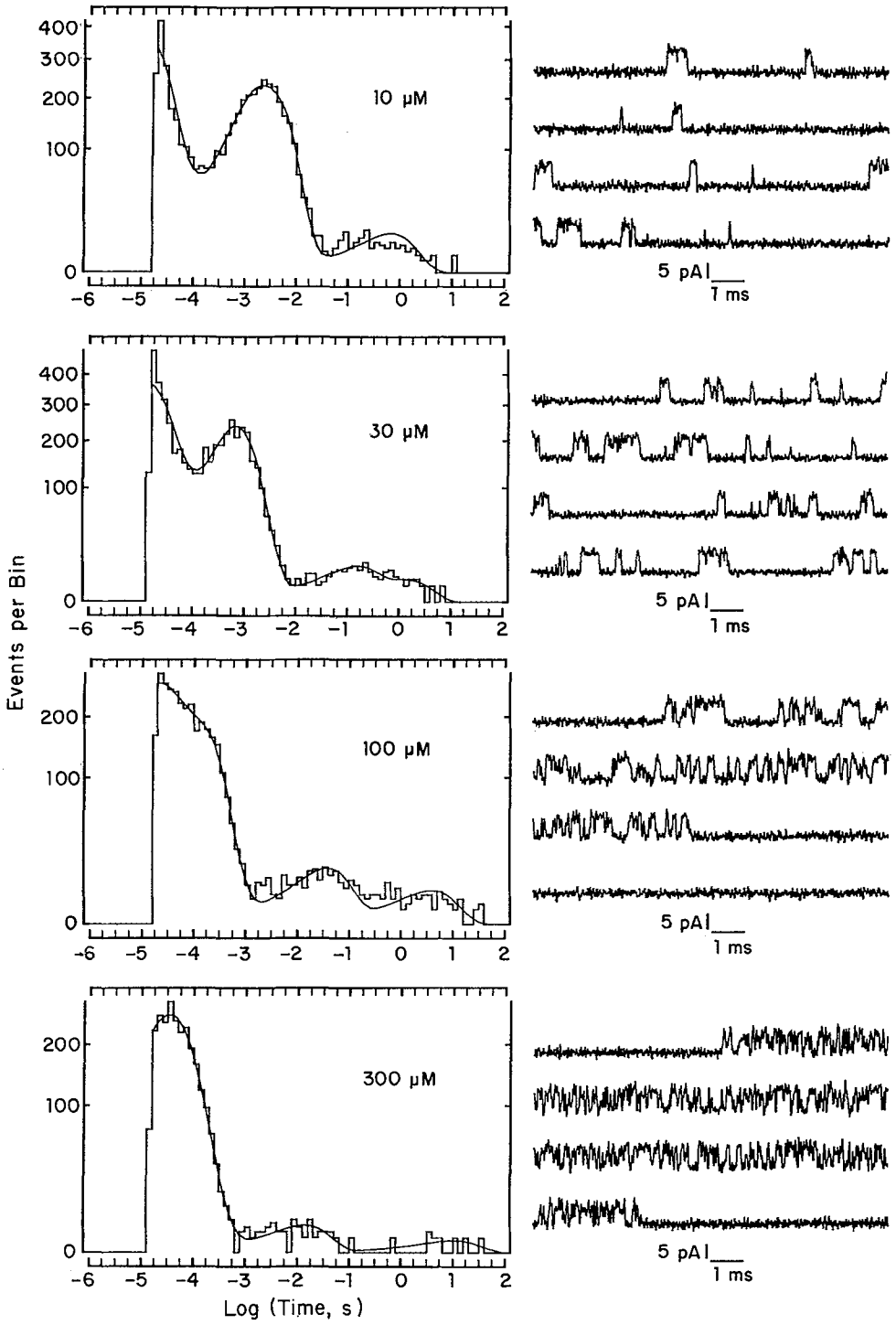

FIGURE 8. Concentration dependence of closed durations for currents recorded at 22°C plus-Ca^{2+}. The data are displayed as in Fig. 6. The fixed parameters, β, k_{-2}, k_{-1}, and k_{-b} are the same as in Fig. 5, *middle*. The fitted parameters are as follows. Top panel (10 μM ACh): $k_{+1} = 6.02 \times 10^7\ M^{-1}s^{-1}$, $k_{+2} = 9.82 \times 10^7\ M^{-1}s^{-1}$, $f_b = 0.133$, $n = 8{,}540$. Second panel (30 μM ACh): $k_{+1} = 6.38 \times 10^7\ M^{-1}s^{-1}$, $k_{+2} = 9.76 \times 10^7\ M^{-1}s^{-1}$, $f_b = 0.206$, $n = 8{,}110$. Third panel (100 μM ACh): $k_{+1} = 7.13 \times 10^7\ M^{-1}s^{-1}$, $k_{+2} = 1.37 \times 10^8\ M^{-1}s^{-1}$, $f_b = 0.33$, $n = 5{,}880$. Bottom panel (300 μM ACh): $k_{+1} = 5.56 \times 10^7\ M^{-1}s^{-1}$, $k_{+2} = 1.25 \times 10^8\ M^{-1}s^{-1}$, $f_b = 0.42$, $n = 4{,}860$.

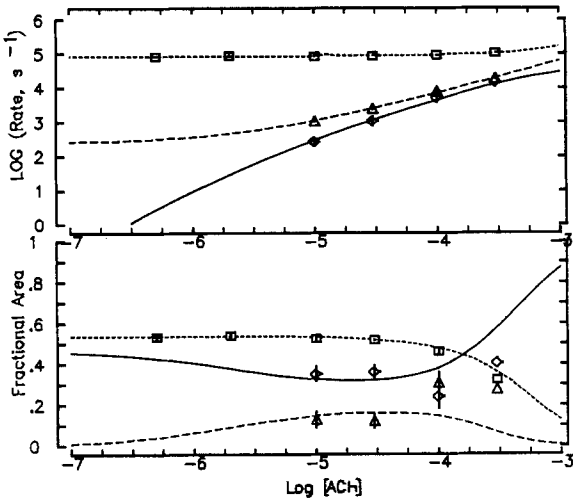

FIGURE 9. Concentration dependence of the rates (*top*) and areas (*bottom*) of the three activation components for the 22°C plus-Ca^{2+} measurements. The data are plotted as in Fig. 7. See Table III for the grand mean rate constants used to plot the theoretical curves.

decreased k_{-2}. The rates of the remaining two components (triangles and diamonds) take on nearly equal values above 30 μM, introducing greater scatter in the fitted areas. Due in part to the slower k_{-1}, the area associated with the triangles peaks at a greater value than without calcium. The β' rate curve (diamonds) is shifted to the left as a result of the twofold increase in affinity of both sites in the presence of calcium.

Fig. 10 displays currents and closed-duration histograms obtained at 12°C with the Ca^{2+}-free solution. Openings are both prolonged and more widely spaced than at 22°C. The brief closures associated with channel block appear more frequently, roughly in proportion to the ACh concentration. These blockages are largely resolved at this temperature, and are better separated from the peak of longer

TABLE III

Summary of Scheme 2 Transition Rates for Three Experimental Conditions

Ca^{2+}-free external solution, 22°C

$$R + A \underset{500\ s^{-1}\ (8.3\ \mu M)}{\overset{6 \times 10^7\ M^{-1}s^{-1}}{\rightleftharpoons}} AR + A \underset{70{,}000\ s^{-1}\ (700\ \mu M)}{\overset{1 \times 10^8\ M^{-1}s^{-1}}{\rightleftharpoons}} A_2R \underset{15{,}000\ s^{-1}}{\overset{22{,}000\ s^{-1}}{\rightleftharpoons}} A_2R^* + A \underset{\sim 70{,}000\ s^{-1}\ (880\ \mu M)}{\overset{\sim 8 \times 10^7\ M^{-1}s}{\rightleftharpoons}} A_2R_{blocked}$$

Plus-Ca^{2+} external solution, 22°C

$$R + A \underset{250\ s^{-1}\ (4.2\ \mu M)}{\overset{6 \times 10^7\ M^{-1}s^{-1}}{\rightleftharpoons}} AR + A \underset{40{,}000\ s^{-1}\ (400\ \mu M)}{\overset{1 \times 10^8 M^{-1}s^{-1}}{\rightleftharpoons}} A_2R \underset{8{,}000\ s^{-1}}{\overset{45{,}000\ s^{-1}}{\rightleftharpoons}} A_2R^* + A \underset{50{,}000\ s^{-1}\ (630\ \mu M)}{\overset{8 \times 10^7 M^{-1}\ s}{\rightleftharpoons}} A_2R_{blocked}$$

Ca^{2+}-free external solution, 12°C

$$R + A \underset{20\ s^{-1}\ (20\ \mu M)}{\overset{1 \times 10^6 M^{-1}s^{-1}}{\rightleftharpoons}} AR + A \underset{20{,}000\ s^{-1}\ (6.7\ mM)}{\overset{3 \times 10^6\ M^{-1}s^{-1}}{\rightleftharpoons}} A_2R \underset{1{,}000\ s^{-1}}{\overset{5{,}000\ s^{-1}}{\rightleftharpoons}} A_2R^* + A \underset{20{,}000\ s^{-1}\ (500\ \mu M)}{\overset{4 \times 10^7 M^{-1}s}{\rightleftharpoons}} A_2R_{blocked}$$

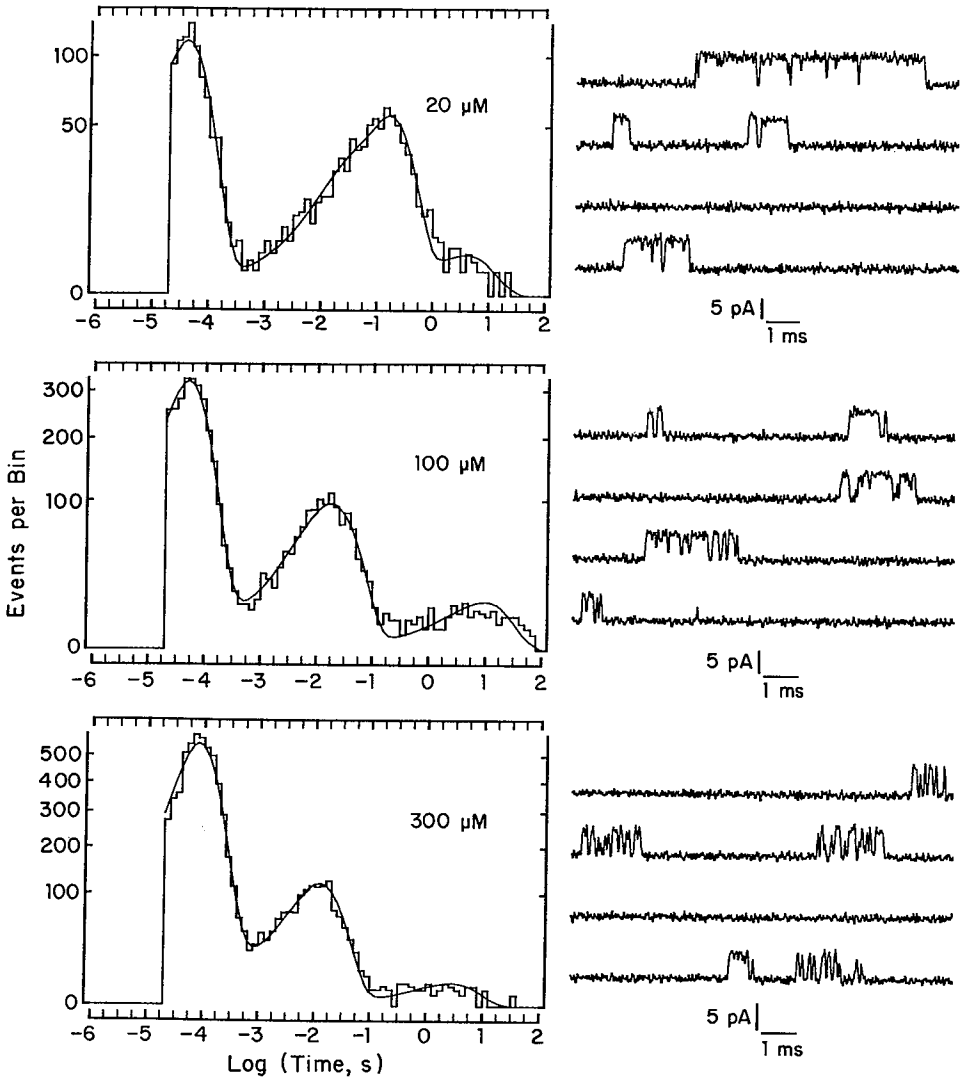

FIGURE 10. Concentration dependence of closed durations for currents recorded at 12°C Ca^{2+}-free. See legend to Fig. 6 for details. The fixed parameters, β, k_{-2}, and k_{-1} are the same ones used in Fig. 5, *bottom*. The fitted parameters are as follows. Top panel (20 μM ACh): $k_{+1} = 1.10 \times 10^6\ M^{-1}s^{-1}$, $k_{+2} = 3.45 \times 10^6\ M^{-1}s^{-1}$, $k_{-b} = 24{,}700\ s^{-1}$, $f_b = 0.537$, $n = 2{,}200$. Middle panel (100 μM ACh): $k_{+1} = 1.06 \times 10^6\ M^{-1}s^{-1}$, $k_{+2} = 3.13 \times 10^6\ M^{-1}s^{-1}$, $k_{-b} = 20{,}100/s^{-1}$, $f_b = 0.709$, $n = 5{,}391$. Bottom panel (300 μM ACh): $k_{+1} = 1.08 \times 10^6\ M^{-1}s^{-1}$, $k_{+2} = 1.48 \times 10^6\ M^{-1}s^{-1}$, $k_{-b} = 12{,}400\ s^{-1}$, $f_b = 0.80$, $n = 9{,}041$.

activation closures. As observed at 22°C, the envelope of activation closures, consisting of two closely spaced components at 20 μM, compresses and moves toward shorter times as the concentration of ACh increases. The fitted curves show that the activation portions of the histograms are well described by Scheme 2.

Fig. 11 shows the concentration dependencies of the activation component parameters measured at 12°C. The lower temperature primarily slows the rates and shifts the rate curves toward higher concentrations. The β' rate curve (solid curve associated with the diamonds) shifts one decade to the right and downward, owing to the decreased affinity of the second site (700 μM to 6.6 mM) and a decrease in β (22,000 to 5,000 s^{-1}). The rate curve associated with the triangles shifts downward 1.5 decades, due mainly to a decrease in k_{-1} from 500 to 20 s^{-1}. Because k_{-1} is decreased the probability of the monoliganded receptor increases, which leads to a greater peak area of the λ_1 component than is seen at 22°C. Neither the area nor the rate associated with A_2R closures (squares) changes with concentration, as observed at 22°C. The data are well described by a single set of Scheme 2 rate constants.

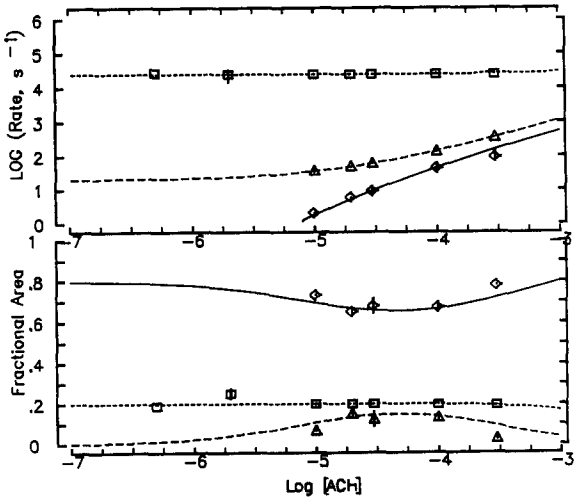

FIGURE 11. Concentration dependence of the rates (*top*) and areas (*bottom*) of the three activation components for the 12°C Ca^{2+}-free measurements. The data are plotted as in Fig. 7. See Table III for the grand mean rate constants used to plot the theoretical curves.

Description of Channel Block at Raised ACh Concentrations

ACh blocks these AChR channels as judged from the concentration-dependent decrease of the mean open duration (compare Figs. 1 and 3), and the parallel increase in frequency of brief closures (Fig. 11). Most of these closures are resolved at 12°C, but are near the limit of resolution at 22°C. Therefore, to extend the analysis of block to greater time resolution, spectral analysis of receptor activity was performed. Greater resolution is expected because spectra include brief subthreshold current pulses not detected in the threshold-crossing analysis. The spectra also serve to check the fitting of well-resolved components of the closed-duration histogram.

Fig. 12 displays corrected difference spectra for currents recorded at a series of ACh concentrations at 12 and 22°C. Spectra were obtained reproducibly out to 40 kHz, with spectral densities well in excess of the expected ion transport noise ($\sim 10^{-30}$ A^2/Hz; Sigworth, 1985). For the 12°C experiments, the 10-μM spectrum appears as a single Lorentzian curve plus a barely visible high frequency component.

As the ACh concentration is increased, the high frequency component increases in magnitude. As expected, the two spectral components arise from the well-separated activation and blocking closed durations (time constants 200–10 ms for activation components and 50 μs for block; see Fig. 10), and the relatively slow channel closing rate (time constant 1 ms; see Fig. 14). Also displayed are spectra for currents elicited by 100 μM ACh at 22°C in the presence and the absence of calcium. Here the spectra appear as two closely spaced Lorentzian curves, in accord with the closer spacing of the activation and blocking components in the closed-duration histograms (Figs. 6 and 8) and the much faster channel-closing rates (time constants 66 and 125 μs in the presence and absence of calcium, respectively). The following sections compare histograms and spectra, with attention turned to analysis of channel block by ACh.

The three parameters of channel block, the mean open duration τ_0, the fraction blocked f_b, and the blocked time ($1/k_{-b}$), can be estimated from analysis of both the power spectrum and the open- and closed-duration histograms. In the histogram analysis the mean open duration is obtained from the rate fitted to the open-duration histogram corrected for missed closings, whereas in the power spectrum it is one determinant of the corner frequency of the low frequency Lorentzian component. According to Scheme 2 the mean open duration τ_0 satisfies

$$1/\tau_0 = \alpha + k_{+b}[\text{ACh}], \tag{2}$$

where the terms are as defined earlier. For both the histogram and the spectrum the fraction blocked f_b is the relative area of the blocking component and is given by

$$f_b = k_{+b}[\text{ACh}]\tau_0. \tag{3}$$

Finally, the unblocking rate is estimated from the time constant of the blocking component in either the histogram or the spectrum. Before comparing histogram and spectral estimates of these parameters, we describe our procedure for fitting power spectra.

Fitted to the experimental spectra in Fig. 12 are theoretical spectra predicted from the dwell time distribution of Scheme 2 (see Appendix II). Nine parameters determine the spectrum: four closed time constants, three areas, the mean open duration, and the single channel current amplitude. The closed-duration components due to desensitization processes do not contribute to the spectrum because the FFT window was positioned to avoid these long closures. Because we wanted to verify the activation rate constants determined from fitting the closed-duration histograms, the activation components (three time constants and three areas) were held constant to the values determined in fitting the closed-duration histograms. We then varied the blocking parameters k_{-b}, f_b, and τ_0; the single channel current amplitude was also varied slightly since it scales the entire spectrum. As seen in Fig. 12, the spectra are well described by the theory, which contains the same activation parameters as the histograms. The spectral fit also gives estimates of the blocking parameters, which in the following sections are compared with blocking parameter estimates obtained from the histograms.

For the 12°C experiments the unblocking rate constant k_{-b} can be determined

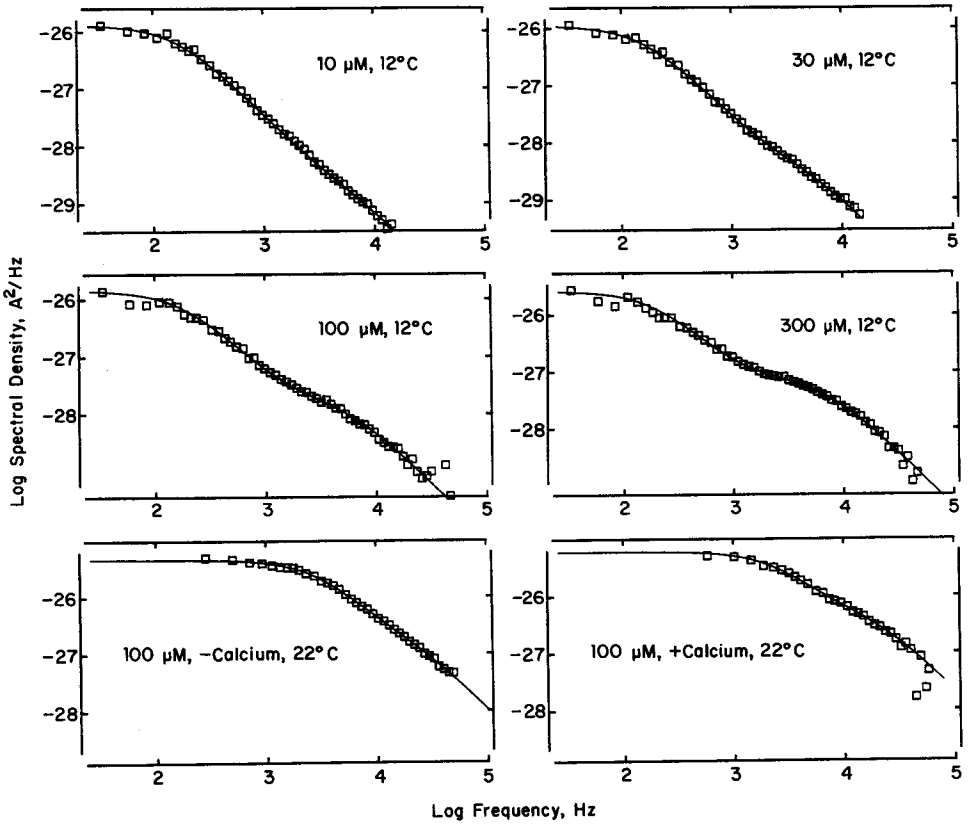

FIGURE 12. Single-channel power spectra. Corrected difference spectra were computed as described under Methods and fitted as described in the text and Appendix II. The upper four spectra were obtained at 12°C with 10, 30, 100, and 300 μM ACh, respectively, whereas the lower two spectra were obtained with 100 μM ACh at 22°C in plus-Ca^{2+} or Ca^{2+}-free solutions. The exponential components for activation were held constant to the values determined in the histogram fitting analysis, while the parameters varied were k_{-b}, fraction blocked (f_b), mean open duration ($1/\tau_0$), and single channel current amplitude (i). The forward blocking rate, k_{+b}, was calculated from text equations 2 and 3. Spectrum 1, 10 μM, 12°C: fitted parameters; $k_{-b} = 37{,}800\ s^{-1}$, $f_b = 0.341$, $1/\tau_0 = 1{,}200\ s^{-1}$, $i = 12.6$ pA, $k_{+b} = 6.21 \times 10^7\ M^{-1}s^{-1}$. Spectrum 2, 30 μM, 12°C: $k_{-b} = 23{,}000\ s^{-1}$, $f_b = 0.573$, $1/\tau_0 = 1{,}200\ s^{-1}$, $i = 6.9$ pA, $k_{+b} = 5.37 \times 10^7\ M^{-1}s^{-1}$. Spectrum 3, 100 μM, 12°C: $k_{-b} = 23{,}100\ s^{-1}$, $f_b = 0.803$, $1/\tau_0 = 1{,}600\ s^{-1}$, $i = 7.06$ pA, $k_{+b} = 6.51 \times 10^7\ M^{-1}s^{-1}$. Spectrum 4, 300 μM, 12°C: $k_{-b} = 20{,}100\ s^{-1}$, $f_b = 0.867$, $1/\tau_0 = 2{,}400\ s^{-1}$, $i = 6.23$ pA, $k_{+b} = 5.22 \times 10^7\ M^{-1}s^{-1}$. Spectrum 5, 100 μM, 22°C, Ca^{2+}-free: $k_{-b} = 99{,}200\ s^{-1}$, $f_b = 0.341$, $1/\tau_0 = 19{,}000\ s^{-1}$, $i = 7.54$ pA, $k_{+b} = 9.86 \times 10^7\ M^{-1}s^{-1}$. Spectrum 6, 100 μM, 22°C, plus-Ca^{2+}: $k_{-b} = 78{,}100\ s^{-1}$, $f_b = 0.463$, $1/\tau_0 = 15{,}000\ s^{-1}$, $i = 6.0$ pA, $k_{+b} = 1.29 \times 10^8\ M^{-1}s^{-1}$.

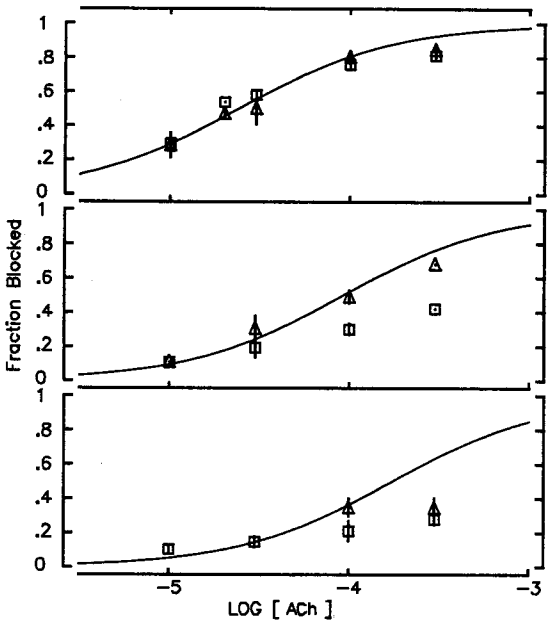

FIGURE 13. Concentration dependence of the fraction blocked f_b. Estimates of f_b were obtained from histogram fitting (squares; see legend to Fig. 5) and from spectral fitting (diamonds; see legend to Fig. 12). *Top*, 12°C, Ca^{2+}-free; *middle*, 22°C, plus-Ca^{2+}; *bottom*, 22°C, Ca^{2+}-free. For top and middle panels Eq. 3 was fitted to the data, yielding the smooth curves and fitted k_{+b} values: 12°C, Ca^{2+}-free, k_{+b} = 5 × 10^7 $M^{-1}s^{-1}$ (fixed α = 1,000 s^{-1}); 22°C, plus-Ca^{2+}, k_{+b} = 1 × 10^8 $M^{-1}s^{-1}$ (fixed α = 15,000 s^{-1}).

directly from the closed-duration histogram because the blockages are well resolved. Although the briefest activation component overlaps the blocking component, its area is much smaller and its rate does not change between 20 and 300 μM (see Fig. 11). The brief activation component is thus not expected to interfere with direct fitting of the blocking component. For the 12°C histogram analysis of the mean k_{-b}

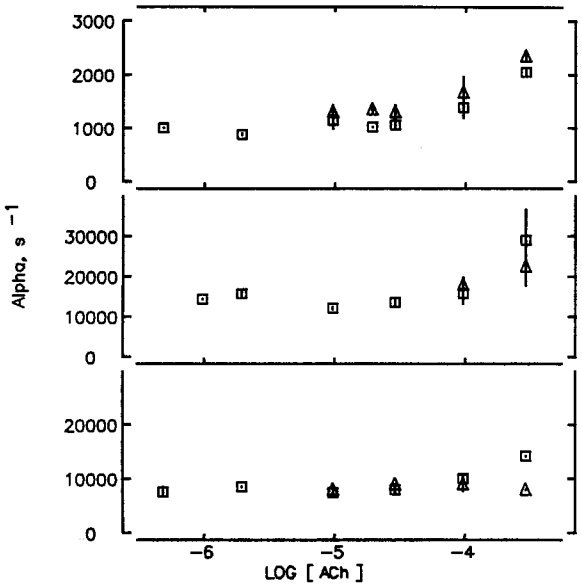

FIGURE 14. Concentration dependence of the apparent α. Values of α were estimated from histogram fitting (squares; see legend to Fig. 5) and from spectral fitting (diamonds). *Top*, 12°C, Ca^{2+}-free; *middle*, 22°C, plus-Ca^{2+}; *bottom*, 22°C, Ca^{2+}-free. Note that α is constant below 30 μM ACh, but increases at higher concentrations.

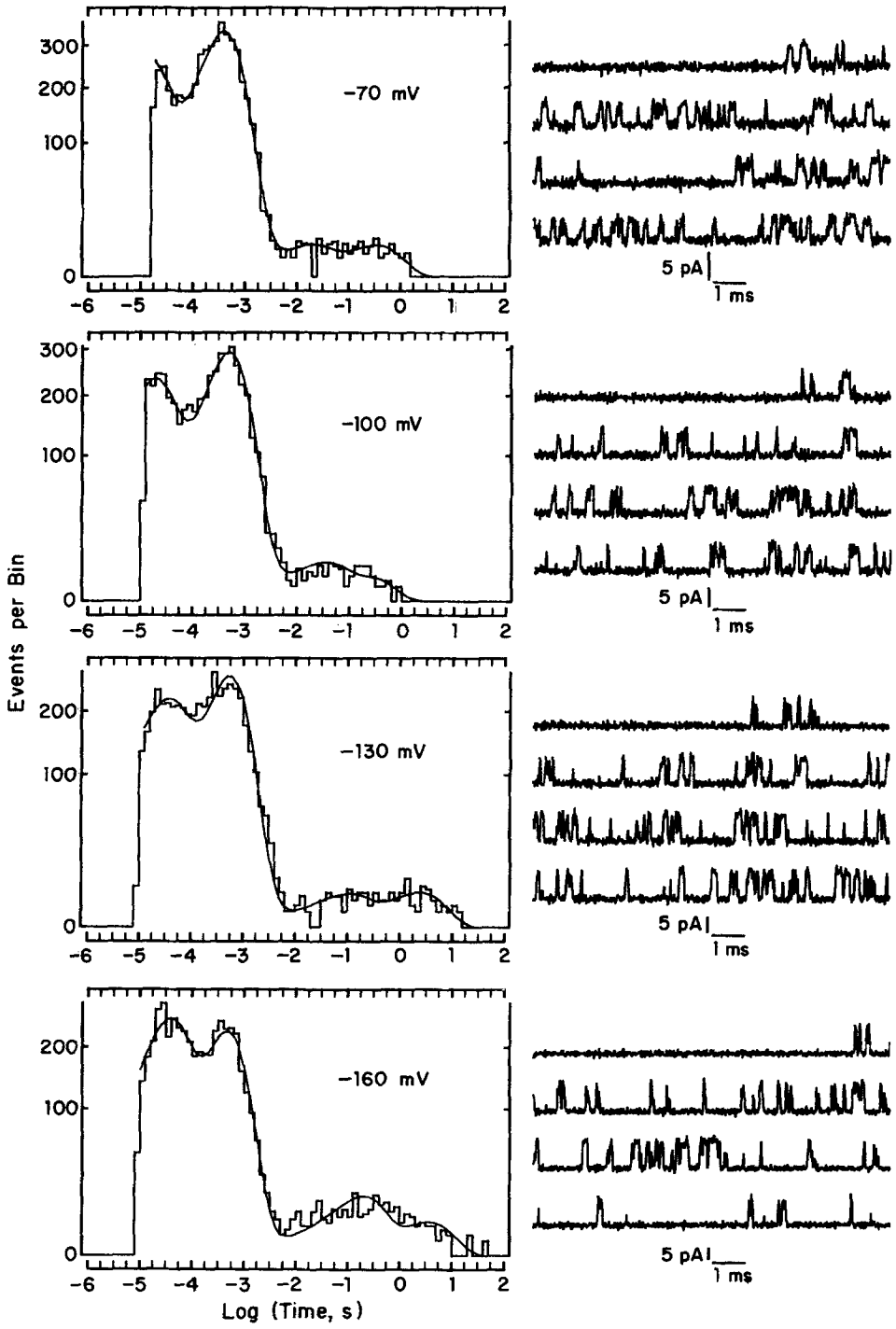
Events per Bin
300
200
100
0
-70 mV
-100 mV
-130 mV
-160 mV
-6 -5 -4 -3 -2 -1 0 1 2
Log (Time, s)
5 pA
1 ms

Figure 15.

is 19,000 ± 4,400 s^{-1} (determined for 20–300 μM ACh). In good agreement with the histogram analysis the spectral analysis reveals a k_{-b} of 19,600 ± 5,600 s^{-1}.

Since at 22°C blockages are brief and more closely overlap the briefest activation component, an analysis similar to that used to estimate k_{-1} was needed to estimate k_{-b} from the closed-duration histograms. The 100-μM histograms were chosen for this analysis because at this concentration blockages are both frequent and reasonably separated from the longer activation closures. k_{-b} was thus assigned various trial values, and k_{+1}, k_{+2}, and f_b were varied so as to maximize the log likelihood. As before, the rates β, k_{-2}, and k_{-1} were held constant to the values determined from the low and intermediate concentration experiments. The series of log likelihood versus k_{-b} plots so obtained yielded the following k_{-b} values: for the Ca^{2+}-free experiments, k_{-b} = 70,000 ± 20,000 s^{-1} (n = 4), and for the plus-Ca^{2+} experiments, k_{-b} = 40,000 ± 15,000 s^{-1} (n = 2). The errors are the ± two log likelihood unit values, which are large due to relatively broad log likelihood versus k_{-b} plots. These k_{-b} values were estimated before doing the full analysis of the activation rates described above, so k_{-b} could be used as a fixed parameter. As might be expected, the spectra give somewhat faster k_{-b} estimates than the histograms: 109,000 ± 32,000 s^{-1} (n = 4) and 50,400 s^{-1} (n = 1) for Ca^{2+}-free and plus-Ca^{2+}, respectively.

The fraction blocked f_b is plotted against ACh concentration in Fig. 13 for the three recording conditions. The squares represent f_b estimated from closed-duration histograms, whereas the triangles represent f_b from power spectra. For the 12°C experiments (Ca^{2+}-free), both the histograms and the spectra reveal a similar f_b at all ACh concentrations. To estimate k_{+b}, Eq. 3 was fitted to the 12°C f_b measurements by holding α constant to the mean low concentration value (1,000 s^{-1}; see Fig. 14) and varying k_{+b}. The data are well described by a forward blocking rate k_{+b} of 4 × 10^7 M^{-1} s^{-1}. At 12°C the calculated dissociation constant for block, k_{-b}/k_{+b}, is 500 μM. Blockages are well resolved at 12°C, and both the histograms and the spectra yield similar f_b estimates.

For the 22°C Ca^{2+}-free experiments, the two estimates of f_b are similar across the concentration range (Fig. 13, *bottom*). However, although f_b increases with concentra-

---

Figure 15. (*opposite*) Voltage dependence of closed durations. Single channel currents and corresponding closed-duration histograms recorded in the presence of 100 μM ACh at 22°C, Ca^{2+}-free. Continuous segments are shown low-pass filtered at 13 kHz (−70 mV) to 20 kHz (−160 mV). The histograms were fitted in a way analogous to that used to determine k_{-1}; k_{-b} was fixed to various values; β, k_{-2}, and k_{-1} were fixed to their previously fitted values; and k_{+1}, k_{+2}, and f_b were varied as described in the legend to Fig. 5 and text. The fitted curves maximize the likelihood for this data set. The blocking parameters are plotted in Fig. 16, while the activation parameters are as follows. Top panel (−70 mV): β = 22,000 s^{-1}, k_{-2} = 70,000 s^{-1}, k_{-1} = 500 s^{-1}, k_{+1} = 5.44 × 10^7 $M^{-1}s^{-1}$, k_{+2} = 1.27 × 10^8 $M^{-1}s^{-1}$. Second panel (−100 mV): β = 18,000 s^{-1}, k_{-2} = 70,000 s^{-1}, k_{-1} = 500 s^{-1}, k_{+1} = 6.10 × 10^7 $M^{-1}s^{-1}$, k_{+2} = 1.17 × 10^8 $M^{-1}s^{-1}$. Third panel (−130 mV): β = 15,000 s^{-1}, k_{-2} = 70,000 s^{-1}, k_{-1} = 500 s^{-1}, k_{+1} = 7.10 × 10^7 $M^{-1}s^{-1}$, k_{+2} = 1.26 × 10^8 $M^{-1}s^{-1}$. Lower panel (−160 mV): β = 12,000 s^{-1}, k_{-2} 70,000 s^{-1}, k_{-1} = 500 s^{-1}, k_{+1} = 9.81 × 10^7 $M^{-1}s^{-1}$, k_{+2} = 1.86 × 10^8 $M^{-1}s^{-1}$. Note that the currents are progressively better resolved as the voltage is made more negative, and in the histograms the barely resolved shoulder at −70 mV moves toward longer times.

tion, it does not saturate, and its concentration dependence is too broad to be described by Eq. 3. Also, the k_{+b} calculated for individual experiments is only slightly greater ($\sim 1 \times 10^8$ M^{-1} s^{-1}) than that measured at 12°C, and it appears to decrease toward the 12°C values with increasing ACh concentration (Table II). In the 22°C experiments it is likely that blockages are too brief for either the histogram or the spectral analysis, and both methods resolve only a portion of them. In addition, the apparent blockages are probably increased in length by smearing with neighboring openings shortened by block. For these 22°C calcium-free experiments our estimate of k_{+b} is thus a lower bound.

For the 22°C experiments carried out in the presence of external calcium, the spectral estimates of f_b are well described by Eq. 3, whereas the histogram estimates show a lower f_b and a broader concentration dependence than can be accounted for by Eq. 3 (Fig. 13, *middle*). Because of its greater frequency resolution, the power

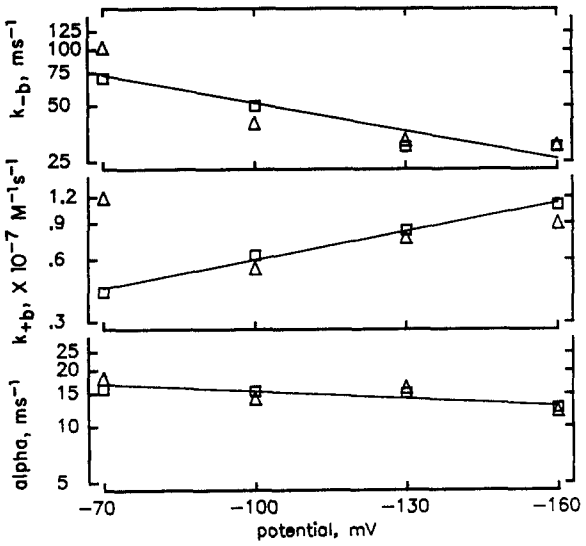

FIGURE 16. Blocking parameters derived from the Fig. 15 histogram fits (squares) or from power spectra (triangles) are plotted against voltage. The straight lines are least-squares fits. *Top,* The unblocking rate, k_{-b}, decreases *e*-fold per 87 mV. *Middle,* The forward blocking rate, k_{+b}, increases *e*-fold per 94.4 mV. *Bottom,* The apparent α decreases *e*-fold per 334 mV.

spectrum seems to more reliably detect blockages for the plus-Ca^{2+} measurements. Fitting Eq. 3 to the spectral estimates yields a k_{+b} of 8.5×10^7 M^{-1} s^{-1} (using a fixed α of 8,000 s^{-1}). At 22°C the calculated blocking dissociation constant is 600 μM.

According to Eq. 2 the mean open duration τ_0 decreases with ACh concentration, but the intrinsic channel closing rate α should be constant. Starting from Eqs. 2 and 3, α was estimated from the measured mean open duration τ_0 and fraction blocked f_b according to

$$\alpha = (1 - f_b)/\tau_0. \tag{4}$$

Fig. 14 shows the resulting spectral and histogram estimates of α plotted against ACh concentration. For the three recording conditions α appears constant up to 30 μM. However at 12°C, where blockages are well resolved, both the histogram and the spectral estimates of α increase at concentrations >30 μM. This increase is also seen

in the histogram estimates for the 22°C plus and minus calcium experiments, although the corresponding spectral analysis shows a smaller increase. The spectral analysis probably misses much of this increase because changes in α produce only subtle changes in the predicted spectrum, whereas readily detectable changes are predicted in the open-duration histogram. Also consistent with an increase in α is the slightly lower than expected fraction blocked seen at 300 μM ACh in Fig. 13, *top*. Since α should not change with concentration, we conclude that a sequential blocking mechanism does not fully describe block of this AChR, and that openings must be shortened at very high concentrations by a mechanism in addition to open channel block. This shortening could occur if blocked channels can close without returning to the open state, as suggested by Neher (1983) for QX-222 block of AChRs on rat myoballs. Alternatively, a long-lived blocked state might be connected to the fast-blocked state but not to any of the other closed states (Ogden and Colquhoun, 1985).

One patch was stable enough to examine the voltage dependence of channel block. The recordings were obtained with 100 μM ACh in the recording pipette, at 22°C in the Ca^{2+}-free solution. Fig. 15 shows currents and the corresponding closed-duration histograms which were fitted by varying the Scheme 2 rate constants as described for the preceding data obtained at -70 mV. In the current traces brief channel closures are progressively better resolved as the voltage is made more negative. This improved resolution is also seen in the closed-duration histograms; the shortest closed-duration component, barely resolved at -70 mV, moves toward longer times at more negative voltages. In fitting the histograms, fixed values of β, k_{-2}, and k_{-1} were used; β and k_{-2} were obtained according to their voltage dependence measured at low ACh concentrations (see Fig. 2), whereas k_{-1} was assumed to be independent of voltage and was assigned the value measured at intermediate ACh concentrations.

The resulting blocking parameters are plotted against voltage in Fig. 16. The squares represent measurements from histograms, whereas the triangles represent those from power spectra. The unblocking rate, k_{-b}, decreases *e*-fold per 87 mV, whereas the forward blocking rate increases *e*-fold per 94 mV. The dissociation constant for block, k_{-b}/k_{+b}, thus decreases *e*-fold per 45 mV. The apparent α shows weak voltage dependence, decreasing *e*-fold per 334 mV, in contrast to the results obtained at low concentrations which show an *e*-fold decrease per 141 mV. The expected voltage dependence of α might be offset by the direct closing of blocked channels at more negative voltages.

DISCUSSION

The experiments described represent the first measurements of the rate constants for the activation pathway of *Torpedo* AChRs. Measurement of these transitions, some of which are very rapid, is made possible by the high temporal resolution of the patch clamp. In addition, the relative simplicity of the *Torpedo* channel kinetics has permitted us to make the most complete determination of activation rate constants for any AChR. For three different recording conditions activation is well described by a four-state linear scheme plus open channel block by ACh. At low ACh concentrations a single brief closed-duration component is observed that yields

estimates of three rates: the channel opening rate β, the dissociation rate of ACh from doubly occupied receptors k_{-2}, and the channel closing rate α. At intermediate concentrations, fitting closely spaced components yields the rate at which ACh dissociates from singly occupied receptors k_{-1}. Finally, over a range of raised ACh concentrations, the fitting analysis discloses the two forward association rates, k_{+1} and k_{+2}. Analysis of single-channel power spectra supports the rate constants estimated from the closed-duration histograms. Overall the rates measured at 22°C seem appropriate for a receptor dedicated to generating sudden brief impulses in the postsynaptic cell. Two surprising but inescapable findings are the widely different affinities of the two ACh binding sites, and the remarkable slowing of the association rates at 12°C.

Scheme 2 has everything needed to describe the kinetics of activation of *Torpedo* receptors over a wide range of ACh concentrations. We have not incorporated desensitization into the scheme, but desensitization closures are so long that we have been able to clearly separate them from the shorter activation closures. Other well-studied receptors, such as those from frog endplate (Colquhoun and Sakmann, 1985), *Xenopus* myotomes (Auerbach and Lingle, 1987), and mouse BC3H-1 cells (Sine and Steinbach, 1986, 1987), exhibit additional closed- and open-duration components not predicted by Scheme 2. For these three AChRs two open-duration components are observed even at high agonist concentrations, and one or more additional closed-duration components are seen at both low (Colquhoun and Sakmann, 1985; Sine and Steinbach, 1986) and high (Auerbach and Lingle, 1987; Sine and Steinbach, 1987) agonist concentrations.

The only other studies of *Torpedo* single-channel current kinetics were carried out with purified AChRs reconstituted in lipid bilayers (Tank et al., 1983; Labarca et al., 1985). Labarca et al. examined the agonist concentration dependence of open durations; closed durations were not studied. Two classes of openings, with time constants of 0.5 and 3.6 ms, were observed between 10 nM and 50 μM ACh at 20°C in solutions containing 0.5 M NaCl and 5 mM Ca^{2+}. The time constants did not change with ACh concentration, but the relative area of the longer openings increased with increasing ACh concentration. Such a concentration dependence of open durations has now been observed in several AChR preparations (Colquhoun and Sakmann, 1985; Papke et al., 1987; Jackson, 1988; Kidokoro and Rohrbough, 1990), and is consistent with long duration openings arising from doubly liganded receptors and at least some of the short duration openings arising from singly liganded receptors. We did not observe a second brief population of openings at 22°C in the presence or the absence of 0.5 mM Ca^{2+}, although at 12°C low concentration experiments (0.5–2 μM ACh, Ca^{2+}-free) showed a small shoulder in the open-duration histograms. We used solutions containing only 1 mM total divalent cations. Perhaps if the Ca^{2+} concentration were increased to 5 mM the open durations might increase further, possibly exposing a second population of brief openings. The general lack of brief openings in our recordings is unfortunate since the concentration dependence of their frequency could give an independent estimate of the high affinity dissociation constant. However, since any brief openings would be rare they are not expected to influence our rate constant estimates.

Significance of the Rate Constants

The following paragraphs consider the functional implications of each rate constant in Scheme 2 (summarized in Table III), and compare them with those estimated in other studies of AChR activation.

In this work the channel opening rate β is estimated from low concentration measurements. β could not be estimated as the limiting opening rate at supersaturating concentrations because the second site binds ACh with very low affinity, and ACh blocks channels in the same concentration range. At 22°C and in the presence of calcium β is estimated to be 45,000 s^{-1} (−70 mV). Such a fast rate means channel isomerization cannot severely limit the rate of receptor activation; doubly occupied receptors thus open with short latency after a pulse of ACh. Colquhoun and Sakmann (1985) estimate a similar value (31,000 s^{-1} at 11°C and −130 mV) from single channel currents recorded at frog endplates, as do Auerbach and Lingle (1987) for the 60-pS channels on cultured *Xenopus* myocytes (range 17,000–56,000 s^{-1} at 23°C and −117 mV). Land et al. (1981) estimates β to be 25,000 s^{-1} (23°C and −100 mV), from the rate of rise of miniature endplate currents at lizard endplates. In the present experiments β shows only weak voltage dependence, decreasing *e*-fold per 145 mV of hyperpolarization. Dionne and Leibowitz (1982) and Sine and Steinbach (1986), who estimate much lower values of β for snake muscle and mouse BC3H-1 receptors, respectively, find a similarly weak but opposite voltage dependence. In this study, removing extracellular calcium decreases β twofold. The increased brief closures in the presence of calcium do not appear to arise from channel block by calcium, as block appears only as a ~25% decrease of the single channel current amplitude (see also Colquhoun and Sakmann, 1985 and Imoto et al., 1986). The apparent Q_{10} for β is 4.5. An estimate of 2.3 has been made from miniature endplate currents in frog muscle (Dwyer, 1981). Comparison of β values for mouse BC3H-1 receptors at 11°C (500 s^{-1}, Sine and Steinbach, 1986, 1987) and at 21°C (8,000 s^{-1}, Papke et al., 1987) suggest even larger Q_{10} values.

Also estimated from low concentration measurements, the dissociation rate of ACh from doubly occupied receptors k_{-2} is 40,000 s^{-1} at 22°C and in the presence of calcium. k_{-2} is thus similar in magnitude to β, so the probability that a channel reopens at low concentration, $\beta/(\beta + k_{-2})$, is ~0.5. Such a fast k_{-2} would also contribute to fast termination of a synaptic response. Colquhoun and Sakmann (1985) and Colquhoun and Ogden (1988) report a lower k_{-2} for frog endplates (16,300 s^{-1} 11°C and −130 mV), as do Auerbach and Lingle (1987) for 60-pS channels on *Xenopus* myocytes (13,000 s^{-1}, 23°C and −117 mV) and Sine and Steinbach (1986) for BC3H-1 receptors (1000 s^{-1}, 11°C, −70 mV). The values quoted, like ours, are raw values, not corrected for the statistics of agonist dissociation (see below). In broad agreement with others, k_{-2} is not voltage dependent (Dionne and Leibowitz, 1982; Colquhoun and Sakmann, 1985; Sine and Steinbach, 1986). Removing external calcium increases k_{-2} about twofold. Of all the activation rate constants, k_{-2} is the least temperature sensitive, showing an apparent Q_{10} of 3.5.

We estimate the channel closing rate α from both low and high concentration experiments where its value is constant up to 30 μM ACh. We propose that the

larger apparent values at higher concentrations arise from direct closing of channels blocked by ACh (Neher, 1983), but we cannot exclude the possibility of a long-lived blocked state connected only to the short-lived blocked state. At 22°C in the presence of calcium, α is 8,000 s^{-1}. A fast α together with a fast k_{-2} would insure rapid termination of a synaptic response. Auerbach and Lingle (1987) report a much slower α for 60-pS channels of *Xenopus* myocytes (1,320 s^{-1}, 23°C). Our opening equilibrium constant, β/α, is weighted less toward open channels (5.3 and 1.75 for plus and minus calcium, respectively) than that of frog endplates ($\beta/\alpha = 43$, Colquhoun and Sakmann, 1985), *Xenopus* myocytes ($\beta/\alpha = 20$, Auerbach and Lingle, 1987), or BC3H-1 cells ($\beta/\alpha = 15$, Sine and Steinbach, 1986, 1987). As is widely observed, α decreases at more negative voltages, although only *e*-fold per 145 mV. Removing external calcium increases α about twofold, as was also found for the much slower receptors of BC3H-1 cells (Sine and Steinbach, 1986). α exhibits a Q_{10} of 15, so at 12°C its value of 1,000 s^{-1} is similar to that for frog endplate receptors (714 s^{-1}, normal Ca^{2+}, 11°C, Colquhoun and Sakmann, 1985), and *Torpedo* receptors expressed in *Xenopus* oocytes (measured open time = 0.61 ms, −100 mV, normal calcium, 20°C, Sakmann et al., 1985; 1,000 s^{-1}, −100 mV, Ca^{2+}-free, 12°C, Sine et al., 1987). Comparison of the results of Sine and Steinbach (1986) with those of Papke et al. (1987) indicates a Q_{10} of only 3 for BC3H-1 receptors. A Q_{10} of 5.3 has been reported for the half power frequency of ACh-induced current fluctuations in embryonic chick myotubes (Sachs and Lecar, 1977).

Our estimates of the association rate constants arise from analysis of closed-duration histograms obtained over a range of high ACh concentrations. We make these estimates without assumptions about binding site symmetry, as the remaining parameters k_{-1} and k_{-2} are estimated from the low and intermediate concentration experiments. At 22°C both association rates are in the range of diffusion-limited values, with $k_{+1} \sim 6 \times 10^7$ and $k_{+2} \sim 1 \times 10^8$ M^{-1} s^{-1}. Capable of both fast binding and fast isomerization, this *Torpedo* receptor is thus ideally suited to delivering fast synaptic responses. Sine and Steinbach (1987), also using estimated values of k_{-1}, k_{-2}, and β, obtained similar association rates (1×10^7 and 1×10^8 M^{-1} s^{-1}, 10°C, −70 mV) for BC3H-1 receptors, although their estimates were not as well constrained by the data as they are for these *Torpedo* receptors. Assuming equivalent binding sites, Auerbach and Lingle (1987) estimate both rates to be $\sim 5 \times 10^8$ $M^{-1}s^{-1}$ for their 40-pS channels, and 1.3 and 2.9×10^8 $M^{-1}s^{-1}$ for their 60-pS channels on *Xenopus* myotomes. Colquhoun and Ogden (1988) estimate both rates to be 8×10^7 $M^{-1}s^{-1}$ (11°C, −95 to −130 mV) from the concentration dependence of the channel open probability measured at frog endplates. In fast mixing experiments with *Torpedo* membranes, Heidmann and Changeux (1979) and Boyd and Cohen (1980) also report diffusion-limited association rates for agonist binding to desensitized receptors. We did not systematically examine the voltage dependence of association rates, but in one patch with 100 μM ACh we found little change in the association rates across a 90-mV range (see legend to Fig. 15). Such insensitivity to voltage is expected for binding of a charged ligand to a site outside the membrane field. Removing extracellular calcium has no effect on the measured association rates. Surprisingly, when the temperature is decreased from 22 to 12°C the two association rates slow to 1×10^6 and 3×10^6 M^{-1} s^{-1}.

The dissociation rate of singly liganded receptors, k_{-1}, could be estimated only at intermediate ACh concentrations (10–30 μM) where all three activation components contribute to the closed-duration histogram. For the three recording conditions, k_{-1} is 350- to 1,000-fold lower than k_{-2}; differences in the two dissociation rate constants thus give rise to most of the difference in binding site affinities. As suggested by Jackson (1988), a slow k_{-1} would increase the sensitivity of the receptor to ACh by stabilizing the singly liganded state, and over a range of high ACh concentrations could also speed the rate of activation after a jump of the ACh concentration. Sine and Steinbach (1987) estimate k_{-1} to be 500 s^{-1} for BC3H-1 AChRs at 11°C, a value similar to ours estimated at 22°C. In the present experiments, removing extracellular calcium increases k_{-1} twofold. k_{-1} is also strongly temperature sensitive, slowing from 500 s^{-1} at 22°C to 20 s^{-1} at 12°C.

For the 12°C measurements both the histogram and the spectral analyses reveal a blocking dissociation constant K_b of ~ 500 μM, with rate constants of 20,000 s^{-1} for k_{-b} and 4×10^7 M^{-1} s^{-1} for k_{+b} (12°C, −100 mV, $-Ca^{2+}$). A similar K_b is estimated for the 22°C experiments with external calcium, but with twofold greater rate constants. The blocking rate constants are thus less temperature sensitive than the activation rate constants. In one patch K_b decreased *e*-fold for 45 mV of hyperpolarization, corresponding to a blocking site 56% of the way through the membrane field. Sine and Steinbach (1984) report a K_b of 2 mM (10°C, −100 mV) for receptors from BC3H-1 cells, and an *e*-fold decrease in K_b per 32 mV for both ACh and suberyldicholine. At frog endplates Ogden and Colquhoun (1985) report a K_b of 1.5 mM (10°C, −110 mV), blocking and unblocking rates of 3.7×10^7 $M^{-1}s^{-1}$ and 56,000 s^{-1}, and a voltage dependence of K_b of *e*-fold per 70 mV. Auerbach and Lingle (1987) report a similar k_{+b} of 3.5×10^7 $M^{-1}s^{-1}$ for 60-pS channels on *Xenopus* myocytes (23°C, −117 mV). ACh thus blocks *Torpedo* channels with about a threefold higher affinity than it does at either frog endplates or BC3H-1 cells; the higher affinity results from a slower unblocking rate for *Torpedo* channels. Neher and Steinbach (1978) report a voltage sensitivity of *e*-fold per 32 mV in the K_b for QX-222 block of AChRs from denervated frog muscle. The similar voltage sensitivities suggest that the site of ACh block for *Torpedo* receptors is at the same position in the membrane field as that for local anesthetic block of denervated frog receptors and agonist block of BC3H-1 receptors.

Different Binding Affinities

Our results show that ACh binds to its two sites with 100- to 300-fold different affinities, and that the affinity difference arises primarily from different rates of ACh dissociation from the two sites. This conclusion was reached by first measuring the dissociation rate constants from closed-duration histograms obtained at low and intermediate ACh concentrations, and then measuring the association rate constants from closed-duration histograms obtained at intermediate and high ACh concentrations. Jackson (1988) also reports different agonist binding affinities for activatable receptors of cultured mouse muscle fibers. His analysis, which is based on a fit of the concentration dependence of the frequency of brief and long duration openings, indicates about a 1,000-fold difference in affinities for carbamylcholine (K_1 of 5 μM and a lower limit K_2 of 3.5 mM; 21°C, −110 mV).

Other studies of AChR activation have been consistent with either independent identical sites or slight positive cooperativity in agonist binding. Macroscopic dose–response measurements do not readily distinguish the two alternatives, although Dionne et al. (1978) suggest some positive cooperativity in frog junctional receptors (600 and 80 μM for carbamylcholine). By estimating rate constants from single-channel current data, Auerbach and Lingle (1987) and Sine and Steinbach (1987) also report modest positive cooperativity in binding for receptors on BC3H-1 cells (50 and 10 μM) and *Xenopus* myotomes (66 and 7 μM for 40-pS channels), respectively. Colquhoun and Ogden (1988), studying frog junctional AChRs, describe their open probability measurements at negative potentials using equivalent binding sites, but their data at positive potentials suggest that the affinities might differ by as much as 10-fold. Since these previous studies would probably have detected the ~100-fold affinity difference we observe in *Torpedo*, we suspect there are differences among species in this respect.

Jackson's (1988) evidence for widely differing binding affinities is different from but complementary to the evidence we present. The receptors he studied show two distinct open-time components, whose concentration dependence implies that they correspond to openings of singly and doubly liganded receptors. Jackson estimates the affinity of the first binding step by measuring the relative frequency of the two types of openings. As discussed earlier, we do not observe a second brief component of open times between 0.5 and 300 μM ACh in our 22°C experiments, and are unable to observe channels at lower concentrations due to the low frequency of events. Instead we measure the dissociation constant of the high affinity site from fitting the broad envelope of activation closed durations recorded at intermediate ACh concentrations. In so doing we also obtain the association and dissociation rate constants k_{+1} and k_{-1}, which yield the high affinity dissociation constant.

Jackson's estimate of the low affinity dissociation constant takes advantage of the slow rate of desensitization at low agonist concentrations, so that early in a recording most of the receptors are activatable. Based on estimates of the number of receptors in a patch and analysis of overlapping channel events, he obtains values for the β' rate in the concentration range of 0.1–20 μM, which extrapolate to a low affinity K_d value for carbamylcholine in the millimolar range. In our experiments we use agonist concentrations closer to the low affinity K_d. The very strong desensitization at these higher concentrations causes channel openings to come in discrete clusters, each representing the activity of a single receptor. We are thus able to measure closed durations at ACh concentrations up to 300 μM, which disclose low affinity dissociation constants of 400, 700, and 6,600 μM under the different recording conditions.

Our experiments do not distinguish whether the two agonist binding sites differ before agonist binds or whether they change affinity after the binding of the first agonist. A change in affinity seems unlikely, because it would require a large reduction in affinity after the first binding step, whereas it is known that the agonist-induced conformational changes leading to channel opening and to desensitization result instead in large increases in affinity of the binding sites. Further, the experiments on BC3H-1 cells of Sine and Taylor (1980, 1981) show that the antagonist dimethyl-*d*-tubocurarine (DMT) binds to the two sites with a 90-fold

difference in affinity, and that the affinities are different before DMT binds. *Torpedo* receptors also exhibit different affinities for curariform antagonists (Neubig and Cohen, 1979; Weiland and Taylor, 1979; Claudio et al., 1987). It is important to note that although the two ACh binding sites are formed by identical alpha subunits, they do not have equivalent contacts with other subunits in the heteropentamer (Karlin, 1987). Initially distinct affinities might well arise from different intersubunit contacts.

To describe receptor activation in terms of initially distinct binding sites, Scheme 1 can be expanded to include two different singly occupied species,

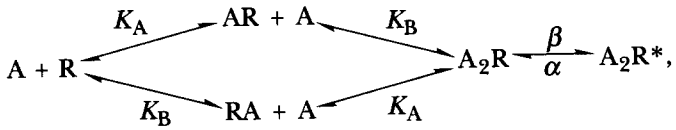

Scheme 3

where the terms are as defined before, and K_A and K_B are the distinguishable dissociation constants. Scheme 3 predicts four closed duration components, compared with three for Scheme 1. However, if K_A and K_B are very different, one of the four components takes on an undetectably small area. For example, using the rate constants obtained for the 22°C Ca^{2+}-free experiments at 100 μM ACh, for Scheme 1 the three predicted rate constants are (in s^{-1}) 6,684, 1,978, and 98,838 with relative areas of 0.042, 0.755, 0.203, respectively. For Scheme 3 the four rate constants are 6,739, 1,965, 100,501, and 85,794 with areas of 0.040, 0.759, 0.199, and 0.0033, respectively. The fourth component of Scheme 3 is therefore too small to detect, and the remaining components do not change appreciably. Thus, when the dissociation constants are very different, as we find experimentally, Scheme 1 (plus channel block) is sufficient to describe the closed-duration distribution. Furthermore, the measured scheme rate constants k_{+1} and k_{-2} correspond directly to the microscopic rate constants.

Dose–response experiments consistently reveal Hill coefficients approaching 2.0 for a wide variety of AChR preparations, including *Torpedo*. It is therefore natural to ask how a receptor with 100-fold different agonist binding affinities produces a cooperative dose–response curve. Fig. 17 shows the predicted dose–response curves for Schemes 1 and 2, given the rate constants determined for the 22°C, plus-Ca^{2+} experiments. For Scheme 1, which contains only activation steps, the dose–response curve (dashed curve) exhibits a Hill coefficient of one at half-maximal activation; of course at threshold concentrations the Hill coefficient approaches 2.0. The apparent dissociation constant equals that of the low affinity binding site. However for Scheme 2, which incorporates channel block, an apparently cooperative response is predicted, and the apparent affinity is greater than that for the low affinity binding site (continuous curve). The symbols plotted in Fig. 17 are rapid flux measurements carried out on *Torpedo* vesicles by Forman and Miller (1988), who obtained a Hill

coefficient of 1.7 for these data. Our predicted dose–response curve closely describes their flux measurements.

Temperature Dependence of the Association Rates

The rate constants for agonist binding decrease sharply when the temperature is lowered from 22°C to 12°C. The decrease is greater for the association than for the dissociation rate at each binding step, greatly reducing the equilibrium sensitivity of receptor at the lower temperature. At 12°C the K_d for the first binding step increases 2.4-fold, while that for the second step increases 11-fold; the K_d for the blocking site, meanwhile, increases only by ~1.4. These changes make for an extremely slow and inefficient synaptic receptor that would activate half-maximally (and also be half blocked) at ~1 mM ACh at 12°C. This temperature is, however, not cold for *Torpedo,* and *Torpedo* AChRs in membrane vesicles show both rapid and sensitive ACh

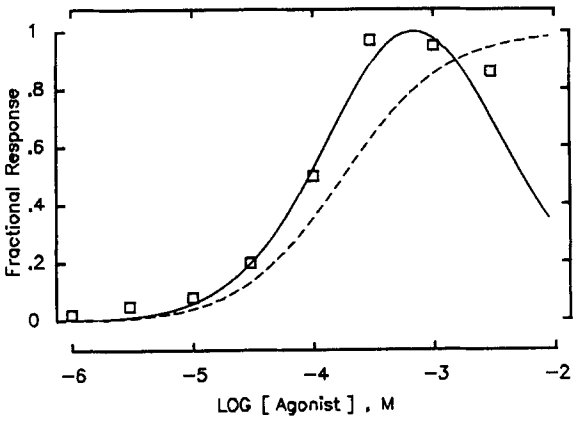

FIGURE 17. Predicted macroscopic dose–response curves for Scheme 1 (dashed curve, no channel block) and Scheme 2 (continuous curve, includes channel block). The symbols are the rapid flux data of Forman and Miller (1988). The parameters used are for the plus-Ca^{2+} data (in $M^{-1}s^{-1}$ or s^{-1}) $k_{+1} = 6 \times 10^7$, $k_{+2} = 1 \times 10^8$, $k_{-1} = 250$, $k_{-2} = 40{,}000$, $\beta/\alpha = 5.6$, $K_b = 1.5$ mM. Note that only the ratio β/α is needed to predict the dose–response curve, and that K_b is the value estimated for 0 mV, assumed for the flux measurements.

responses even at lower temperatures (the data of Forman and Miller shown in Fig. 17 were obtained at 5°C). The remarkably slow rates at 12°C appear to result from the mouse fibroblast expression system: RNA transcribed from the same cDNAs and injected into *Xenopus* oocytes yields receptors with ~10-fold higher sensitivity to ACh at this temperature (S. Sine, unpublished observations).

Although differences in posttranslational processing might explain the anomalous temperature dependence of the *Torpedo* AChRs in fibroblasts, we favor the hypothesis that a reduction in membrane fluidity in this temperature range slows the various activation steps in the AChR. But how could "freezing" of the lipid matrix affect the affinity of binding sites outside the membrane, in particular causing a 60-fold reduction in the association rate k_{+1} from the diffusion-limited value seen at 22°C? We suggest that agonist binding depends on internal motions of the AChR molecule; these motions could in turn be damped by the lipid matrix so that binding

is greatly slowed to a receptor in a frozen membrane. An effect of this sort has been described by Beece et al. (1980) in myoglobin, where the viscosity of the aqueous solvent is shown to have a strong effect on the rate of transitions that occur deep within the protein.

APPENDIX

I. Correction for Missed Events

The channel open and closed dwell times measured in this study were often short enough that, in the process of determining rate constants, a correction had to be applied to account for the effects of missed events. In our data there appears to be only one open state, so that the correction for the open times is straightforward in principle. First an estimate is made, by extrapolation, of the true number of closed durations; then the total open time in a run is divided by this number to yield the "true" mean open time. The difficulty lies in estimating the true number of closed events, which in turn requires an estimate of the mean open time so that the probability of missed openings can be taken into account. As described in Methods, we repeated three times the fitting of the open and closed time distributions with missed-event corrections to allow the estimated probability of missed events to converge.

The presence of multiple closed states makes the correction of the closed time distribution more complicated. Various authors have considered this problem and have presented solutions for schemes ranging from simple two-state to general multistate schemes (see, for example, Roux and Sauvé, 1985 and Blatz and Magleby, 1986). We describe here the approach used for this study, which is essentially an approximation to the exact solution given by Roux and Sauvé and which is suited only to schemes with one open state. More elegant approximations have been presented by Milne et al. (1988); a more general theory has also been developed along the lines described here (Crouzy and Sigworth, 1990) that yields better approximations with less computation.

As in previous analyses of this problem, we assume a well-defined dead time δ, such that all open or closed dwell times shorter than δ are not detected, and all longer dwells are detected. Consider a sequence of channel-closed intervals t_0, t_1, ... with interspersed brief open intervals t'_0, t'_1, ... which have a probability p_m of being missed. With probability $(1 - p_m)$ the first closed event will be found to have duration t_0 since it will be followed by an open interval t'_0 that is detected. However, with probability $p_m(1 - p_m)$, t'_0 will be missed but the second open interval t'_1 will be detected; the observed closed interval will then be $t_0 + t'_0 + t_1$. In general, the probability of missing n open intervals is

$$P_{(n)} = p_m^n(1 - p_m),$$

and the apparent duration of the closed interval when n openings are missed is

$$T_{(n)} = t_0 + \sum_{i=1}^{n} t''_{i-1} + t_i,$$

where by t''_0, t''_1, ... we represent open intervals that are shorter than δ, i.e., that are conditionally distributed (Milne et al., 1988). The goal is to compute a probability density function for the observed closed times, which can be computed as a sum of the pdf's of the $T_{(n)}$ weighted by the corresponding probabilities $P_{(n)}$. Let f be the pdf of the closed times and f' be that of the open times. Since the pdf of a sum of random variables is obtained as the

convolution of the pdf's of each variable, we could in principle obtain the pdf's $F_{(n)}$ of the $T_{(n)}$ by repeated convolutions of f and f':

$$F_{(0)}(t) = f(t)$$

$$F_{(1)}(t) = f(t) * f'(t) * f(t)$$

$$F_{(2)}(t) = f(t) * f'(t) * f(t) * f'(t) * f(t),$$

and so on. In writing these equations we make use of the fact that there is only one open state, so that by the Markov property of the kinetic process the successive dwell times are independent random variables (Colquhoun and Hawkes, 1977). The desired pdf of apparent closed intervals would then be given by

$$f_{\text{app}}(t) = \sum_{i=0}^{\infty} P_{(i)} F_{(i)}(t). \tag{A1}$$

In our evaluation of f_{app} we truncated the sum after $i = 2$, leaving an error on the order of p_m^3. The approximate evaluation of the $F_{(i)}$ was done in the following manner. Given that $f(t)$ is the sum of m exponential terms,

$$f(t) = \sum_{i=1}^{m} a_i \lambda_i \exp(-\lambda_i t),$$

we note that $F_{(1)}$ and $F_{(2)}$ can be written as

$$F_{(1)}(t) = \sum_{i=1}^{m} \sum_{j=1}^{m} a_i a_j G_{ij}(t)$$

$$F_{(2)}(t) = \sum_{i=1}^{m} \sum_{j=1}^{m} \sum_{k=1}^{m} a_i a_j a_k H_{ijk}(t), \tag{A2}$$

where $G_{ij}(t)$ is the result of the convolution of the i^{th} and j^{th} exponential components together with $f'(t)$; i.e.,

$$G_{ij}(t) = \int_{u=0}^{t} \int_{v=0}^{u} \lambda_i \lambda_j \exp(\lambda_i v) \exp[\lambda_j (u - v)] f'(t - u)\, dv\, du,$$

and H_{ijk} is the analogous fourfold convolution. Rather than evaluating these, we approximated G and H by single-exponential probability densities having the same mean value,

$$G_{ij}(t) \approx \exp[-t/(\tau_i + \tau_j + \delta)]$$

and

$$H_{ijk}(t) \approx \exp[-t/(\tau_i + \tau_j + \tau_k + 2\delta)], \tag{A3}$$

where $\tau_\mu = 1/\lambda_\mu$ and we have assumed that the mean of the missed open times t_i' is δ.

Using this theory, we implemented the correction for missed open events within the process of fitting distributions (see Blatz and Magleby, 1986). For a given set of rate constants the theoretical closed-time pdf was computed; from it and an estimate of p_m (obtained from iterated fits to the open-duration distribution) f_{app} was computed by summing the first three terms of Eq. A1 by evaluating Eqs. A2 and A3. The likelihood was then computed from the

dwell time data and f_{app}, and the process repeated to find the rate constants maximizing it. Since p_m was <0.3 in every case, truncating the series is expected to result in negligible errors on the order of $p_m^3 \approx 0.03$. The errors introduced by the approximations (Eq. A3) were minor since a comparison of the resulting f_{app} with those computed using better approximations (Crouzy and Sigworth, 1990) gave indistinguishable results.

It has been pointed out (Colquhoun and Sigworth, 1983; Yeo et al., 1988) that more than one set of rate constants can yield the same observed dwell time distribution when events are missed. The alternative sets of rate constants are much faster, and correspond to values of p_m approaching unity. The relatively low values of p_m that we obtained from our iterated fits were consistent with the general appearance of the recordings, which suggested a low p_m. The systematic variation of fitted parameters with ACh concentration (e.g., Figs. 7, 9, and 11) also argues that our relatively small corrections did not yield anomalous estimates of rates.

II. Prediction of the Power Spectrum from Open and Closed Time Distributions

It is well known that, given the set of transition rates among the states of a kinetic scheme for channel gating, both the dwell time distributions and the power spectral density of the channel current fluctuations can be predicted (Colquhoun and Hawkes, 1977; 1982). For the present study we wanted to relate our power spectrum observations directly to the channel dwell time distributions without reference to the underlying transition rates. We present here the theory that allows the power spectrum to be computed directly from the dwell time distributions.

The autocovariance function $c(\tau)$ is related to the power sepctrum $S(f)$ by the inverse Fourier transformation,

$$c(\tau) = \int_{-\infty}^{\infty} S(f) e^{j2\pi f\tau}\, df. \tag{1}$$

The autocovariance of steady-state channel activity with mean open probability p is also given by

$$c(\tau) = Ni^2(pp_1(\tau) - p^2),$$

where N is the number of channels, i is the single-channel current, and $p_1(\tau)$ is the conditional probability of a channel being open at time τ, given that it is open at time 0. For stationary channel activity (as assumed here) $p_1(\tau)$ is an even function of τ. However, for now we consider only positive τ and define the one-sided conditional probability

$$p_{1+}(\tau) = \begin{cases} p_1(\tau), & \tau \geq 0 \\ 0, & \tau < 0, \end{cases}$$

which is given by

$$p_{1+}(\tau) = F'(\tau) + \int_0^{\infty}\int_0^{\infty} f(t_1)g(t_2)F'(\tau - t_1 - t_2)\, dt_1\, dt_2, + \ldots, \tag{2}$$

where $F'(\tau)$ = Prob [channel open time $> \tau$] is the probability distribution (survivor) function for channel open times, assumed to be zero for negative arguments; f is the probability density function of open times and g the probability density of closed times. The first term of Eq. 2 represents the probability that a channel remains open during the entire interval τ. The second term is the probability of the channel closing once and reopening, being open at τ; it is obtained by integrating the probability of closing after an open dwell time t_1, reopening after a closed time t_2, and then remaining open until τ. Successive terms of the sum represent the cases of two, three, or more closings interposed in the interval $(0, \tau)$.

The Laplace transform of Eq. 2 is

$$\hat{p}_{1+}(s) = \hat{F}'(s) \sum_{n=0}^{\infty} [\hat{f}(s)\hat{g}(s)]^n = \frac{\hat{F}'(s)}{1 - \hat{f}(s)\hat{g}(s)}, \tag{3}$$

where $\hat{p}_{1+}$, $\hat{E}'$, $\hat{f}$, and $\hat{g}$ are the Laplace transforms of the corresponding functions, and we make use of the fact that convolutions in the time domain become products in the Laplace transform domain. The Laplace transform of the (one-sided) autocovariance function is then

$$\hat{c}_+(s) = Ni^2p[\hat{p}_{1+}(s) - p/s], \tag{4}$$

and $c(\tau)$, which is an even function, is obtained by inverting the Laplace transform,

$$\begin{aligned} c(\tau) &= c_+(\tau) + c_+(-\tau) \\ &= \int_{-\infty}^{\infty} [\hat{c}_+(j2\pi f) + \hat{c}_+(-j2\pi f)]e^{j2\pi f\tau}\, d\tau \\ &= \int_{-\infty}^{\infty} 2\ \mathrm{Re}[\hat{c}_+(j2\pi f)]e^{j2\pi f\tau}\, d\tau. \end{aligned} \tag{5}$$

Finally, comparison with Eq. 1 and the uniqueness of the Fourier transform implies that

$$S(f) = 2\ \mathrm{Re}[\hat{c}_+(j2\pi f)].$$

The final result is obtained by substituting with Eq. 5 and taking the real part:

$$S(f) = Ni^2p\ \mathrm{Re}\left\{\frac{\hat{F}'(j2\pi f)}{1 - \hat{f}(j2\pi f)\hat{g}(j2\pi f)}\right\}. \tag{6}$$

This function is readily evaluated when the functions F', f, and g are sums of exponentials. As an example, consider the simple case of a simple two-state channel,

$$\text{closed} \underset{\beta}{\overset{\alpha}{\rightleftharpoons}} \text{open}.$$

The probability functions are:

$$\begin{aligned} p &= \alpha/(\alpha + \beta) \\ F'(\tau) &= e^{-\beta\tau} \\ f(\tau) &= \beta e^{-\beta\tau} \\ g(\tau) &= \alpha e^{-\alpha\tau}, \end{aligned}$$

and have the transforms

$$\begin{aligned} \hat{F}'(s) &= 1/(s + \beta) \\ \hat{f}(s) &= \beta/(s + \beta) \\ \hat{g}(s) &= \alpha/(s + \alpha). \end{aligned}$$

Substitution into Eq. 6 yields the standard result for the power spectrum,

$$S(f) = \frac{\alpha\beta}{\alpha + \beta} \frac{1}{(2\pi f)^2 + (\alpha + \beta)^2}.$$

We thank Dr. Serge Crouzy for help in checking the approximations in our analysis.

This work was supported by grant HL-38156 from the National Institutes of Health.

Original version received 19 July 1989 and accepted version received 16 February 1990.

REFERENCES

Adams, P. R. 1975. An analysis of the dose-response curve at voltage-clamped frog endplates. *Pflügers Archiv.* 360:145–153.

Auerbach, A., and C. J. Lingle. 1987. Activation of the primary kinetic modes of large- and small-conductance cholinergic ion channels in *Xenopus* myocytes. *Journal of Physiology.* 393:437–466.

Beece, D., L. Eisenstein, H. Frauenfelder, D. Good, M. C. Marden, L. Reinisch, A. H. Reynolds, L. B. Sorensen, and K. T. Yue. 1980. Solvent viscosity and protein dynamics. *Biochemistry.* 19:5147–5157.

Blatz, A. L., and K. L. Magleby. 1986. Correcting single channel data for missed events. *Biophysical Journal.* 49:967–980.

Boyd, N. D., and J. B. Cohen. 1980. Kinetics of binding of ^{3}H-acetylcholine to *Torpedo* postsynaptic membranes: association and dissociation rate constants by rapid mixing and ultrafiltration. *Biochemistry.* 19:5353–5458.

Caceci, M. S., and W. P. Cacheris. 1984. Fitting curves to data: the simplex algorithm is the answer. *Byte.* 9:340–348.

Claudio, T., W. N. Green, D. S. Hartmann, D. Hayden, H. L. Paulson, F. J. Sigworth, S. M. Sine, and A. Swedlund. 1987. Genetic reconstitution of functional acetylcholine receptor channels in mouse fibroblasts. *Science.* 238:1688–1694.

Cohen, J. B., M. Weber, and J. P. Changeux. 1974. Effects of local anesthetics and calcium on the nicotinic receptor protein from *Torpedo marmorata. Molecular Pharmacology.* 10:904–932.

Colquhoun, D., and A. G. Hawkes. 1977. Relaxations and fluctuations of membrane currents that flow through drug operated channels. *Proceedings of the Royal Society of London B.* 199:231–262.

Colquhoun, D., and A. G. Hawkes. 1981. On the stochastic properties of single ion channels. *Proceedings of the Royal Society of London B.* 211:205–235.

Colquhoun, D., and A. G. Hawkes. 1982. On the stochastic properties of bursts of single ion channel openings and of clusters of bursts. *Philosophical Transactions of the Royal Society of London B.* 300, 1–59.

Colquhoun, D., and D. Ogden. 1988. Activation of ion channels in the frog endplate by high concentrations of acetylcholine. *Journal of Physiology.* 395:131–159.

Colquhoun, D., and B. Sakmann. 1985. Fast events in single channel currents activated by acetylcholine and its analogs at the frog muscle endplate. *Journal of Physiology.* 369:501–557.

Colquhoun, D., and F. J. Sigworth. 1983. Fitting and statistical analysis of single channel records. *In* Single Channel Recordings. B. Sakmann and E. Neher, editors. Plenum Publishing Corp., New York. 191–264.

Crouzy, S. C., and F. J. Sigworth. 1990. Yet another approach to the dwell-time omission problem of single-channel analysis. *Biophysical Journal.* In press.

Dionne, V. E., and M. A. Leibowitz. 1982. Acetylcholine receptor kinetics. A description of single channel currents at snake neuromuscular junctions. *Biophysical Journal.* 39:253–261.

Dionne, V. E., J. H. Steinbach, and C. F. Stevens. 1978. An analysis of the dose-response relationship at voltage-clamped frog neuromuscular junctions. *Journal of Physiology.* 218:421–444.

Dreyer, F., K. Peper, and R. Sterz. 1978. Determination of dose-response curves by quantitative iontophoresis at the frog neuromuscular junction. *Journal of Physiology.* 281:395–419.

Dwyer, T. M. 1981. The rising phase of miniature endplate current at the frog neuromuscular junction. *Biochimica et Biophysica Acta.* 646:51–60.

Forman, S. A., and K. W. Miller. 1988. High acetylcholine concentrations cause rapid inactivation before fast desensitization in nicotinic acetylcholine receptors from *Torpedo. Biophysical Journal.* 54:149–158.

Hamill, O. P., A. Marty, E. Neher, B. Sakmann, and F. J. Sigworth. 1981. Improved patch clamp technique for high resolution current recording from cells and cell-free membrane patches. *Pflügers Archiv.* 391:85–100.

Heidmann, T., and J. P. Changeux. 1979. Fast kinetic studies on the interaction of a fluorescent agonist with the membrane-bound acetylcholine receptor from *Torpedo marmorata. European Journal of Biochemistry.* 94:255–279.

Imoto, K., C. Busch, B. Sakmann, M. Mishina, T. Konno, J. Nakai, H. Bujo, Y. Mori, K. Fukuda, and S. Numa. 1988. Rings of negatively charged amino acids determine the acetylcholine receptor conductance. *Nature.* 335:645–648.

Imoto, K., C. Methfessel, B. Sakmann, M. Mishina, Y. Mori, T. Konno, K. Fukuda, M. Kurasaki, H. Bujo, Y. Fujita, and S. Numa. 1986. Location of a δ-subunit region determining ion transport through the acetylcholine receptor channel. *Nature.* 324:670–674.

Jackson, M. B. 1988. Dependence of acetylcholine receptor channel kinetics on agonist concentration in cultured mouse muscle fibres. *Journal of Physiology.* 397:555–583.

Jackson, M. B. 1989. Perfection of a synaptic receptor: the kinetics and energetics of the acetylcholine receptor. *Proceedings of the National Academy of Sciences.* 86:2199–2203.

Karlin, A. 1987. Molecular biophysics: going round in receptor circles. *Nature.* 329:286–287.

Kidokoro, Y., and J. Rohrbough. 1990. Kinetics of acetylcholine receptor channels in *Xenopus* myocyte culture: brief openings, brief closings and slow desensitization. *Journal of Physiology.* 425:227–244.

Labarca, P., M. S. Montal, J. Lindstrom, and M. Montal. 1985. The occurrence of long openings in the purified cholinergic receptor channel increases with acetylcholine concentration. *Journal of Neuroscience.* 5:3409–3413.

Land, B., E. Salpeter, and M. Salpeter. 1981. Kinetic properties for acetylcholine interaction in intact neuromuscular junctions. *Proceedings of the National Academy of Sciences.* 78:7200–7204.

Leonard, R. J., C. G. Labarca, P. Charnet, N. Davidson, and H. Lester. 1988. Evidence that the M2 membrane spanning region lines the ion channel pore of the nicotinic receptor. *Science.* 242:1578–1581.

Milne, R. K., G. F. Yeo, R. O. Edeson, and B. W. Madsen. 1988. Stochastic modelling of a single ion channel: an alternating renewal approach with application to limited time resolution. *Proceedings of the Royal Society of London B.* 233:247–292.

Neher, E. 1983. The charge carried by single-channel currents of rat cultured muscle cells in the presence of local anesthetics. *Journal of Physiology.* 339:663–678.

Neher, E., and J. H. Steinbach. 1978. Local anesthetics transiently block currents through single acetylcholine receptor channels. *Journal of Physiology.* 277:153–176.

Neubig, R. R., and J. B. Cohen. 1979. Equilibrium binding of ^{3}H-tubocurarine and ^{3}H-acetylcholine by *Torpedo* postsynaptic membranes: stoichiometry and ligand interactions. *Biochemistry.* 18:5464–5475.

Ogden, D. C., and D. Colquhoun. 1985. Ion channel block by acetylcholine, carbachol, and suberyldicholine at the frog neuromuscular junction. *Proceedings of the Royal Society of London B.* 225:329–355.

Papke, R. L., G. Millhauser, Z. Lieberman, and R. E. Oswald. 1987. Relationships of agonist properties to the single channel kinetics of nicotinic acetylcholine receptors. *Biophysical Journal.* 53:1–10.

Paulson, H., and T. Claudio. 1990. Temperature-sensitive expression of *Torpedo* and mammalian-*Torpedo* hybrid AChR in mammalian muscle cells. *Journal of Cell Biology.* 110:1705–1717.

Roux, B., and R. Sauvé. 1985. A general solution to the time interval omission problem applied to single channel analysis. *Biophysical Journal.* 48:149–158.

Sachs, F., and H. Lecar. 1977. Acetylcholine-induced current fluctuations in tissue-cultured muscle cells under voltage clamp. *Biophysical Journal.* 17:129–143.

Sakmann, B., C. Methfessel, M. Mishina, T. Takahashi, T. Takai, M. Kurasaki, K. Fukuda, and S. Numa. 1985. Role of acetylcholine receptor subunits in gating of the channel. *Nature.* 318:538–543.

Sakmann, B., J. Patlak, and E. Neher. 1980. Single acetylcholine activated channels show burst kinetics in the presence of desensitizing concentrations of agonist. *Nature.* 286:71–73.

Sigworth, F. J. 1983. An example of analysis. *In* Single Channel Recording. B. Sakmann and E. Neher, editors. Plenum Publishing Corp. New York. 301–321.

Sigworth, F. J. 1985. Open channel noise. I. Noise in acetylcholine receptor currents suggests conformational fluctuations. *Biophysical Journal.* 47:709–720.

Sigworth, F. J., and S. M. Sine. 1987. Data transformations for improved display and fitting of single-channel dwell time histograms. *Biophysical Journal.* 52:1047–1054.

Sine, S. M., T. Claudio, and F. J. Sigworth. 1987. Functional properties of *Torpedo* acetylcholine receptors genetically reconstituted in mouse fibroblasts. *Biophysical Journal.* 53:637*a*. (Abstr.)

Sine, S. M., and J. H. Steinbach. 1984. Agonists block currents through acetylcholine receptor channels. *Biophysical Journal.* 46:277–284.

Sine, S. M., and J. H. Steinbach. 1986. Activation of acetylcholine receptors on clonal mammalian BC3H-1 cells by low concentrations of agonist. *Journal of Physiology.* 373:129–162.

Sine, S. M., and J. H. Steinbach. 1987. Activation of acetylcholine receptors on clonal mammalian BC3H-1 cells by high concentrations of agonist. *Journal of Physiology.* 385:325–359.

Sine, S. M., and P. Taylor. 1979. Functional consequences of agonist-mediated state transitions in the cholinergic receptor: studies on cultured muscle cells. *Journal of Biological Chemistry.* 254:3315–3325.

Sine, S. M., and P. Taylor. 1980. The relationship between agonist occupation and the permeability response of the cholinergic receptor revealed by bound cobra-α-toxin. *Journal of Biological Chemistry.* 255:10144–10156.

Sine, S. M., and P. Taylor. 1981. Relationship between reversible antagonist occupancy and the functional capacity of the acetylcholine receptor. *Journal of Biological Chemistry.* 256:6692–6699.

Tank, D. W., R. L. Huganir, P. Greengard, and W. W. Webb. 1983. Patch recorded single-channel currents of the purified and reconstituted *Torpedo* acetylcholine receptor. *Proceedings of the National Academy of Sciences.* 80:5129–5133.

Weber, M., and J. P. Changeux. 1974. Binding of *Naja nicricollis* ^{3}H-α-toxin to membrane fragments from *Electrophorus* and *Torpedo* electric organs: effect of cholinergic agonists and antagonists on the binding of α-neurotoxin. *Molecular Pharmacology.* 10:15–34.

Weiland, G., and P. Taylor. 1979. Ligand specificity of state transitions in the cholinergic receptor: behavior of agonists and antagonists. *Molecular Pharmacology.* 15:197–212.

Yeo, G. F., R. K. Milne, R. O. Edeson, and B. W. Madsen. 1988. Statistical inference from single channel records: a two-state Markov model with limited time resolution. *Proceedings of the Royal Society of London B.* 235:63–94.